

Movement of spherical colloid particles carried by flow in tubes of periodically varying diameter

František Slanina*

Institute of Physics, Academy of Sciences of the Czech Republic, Na Slovance 2, CZ-18221 Praha, Czech Republic (Received 14 February 2018; revised manuscript received 19 September 2018; published 8 January 2019)

We provide analytical formulas for the movement of spherical particles in a corrugated tube, in the approximation of small amplitude of the tube diameter variation. We calculate how the particle is pushed toward the wall at some places and pulled off the wall at others. We show that this effect causes rectification of the particle movement, when the direction of the fluid flow is alternated, thus leading to the hydrodynamic ratchet effect. We propose such scheme as a particle-separation device.

DOI: [10.1103/PhysRevE.99.012604](https://doi.org/10.1103/PhysRevE.99.012604)**I. INTRODUCTION**

One of the key tasks in microfluidics [1,2] is separation of tiny particles according to their size, shape, rigidity, and other physical properties [3–8]. Applications range from colloids [9] to separation of cancer cells flowing in human blood [10]. Soft matter in narrow pores is a very intriguing field in general [11].

There are numerous approaches to microparticle sorting relevant to microfluidics. Let us first mention the microfluidic Brownian ratchets [12,13], which combine Brownian motion, alternating fluid flow, and mirror-asymmetric geometry of the channel, to produce rectification of otherwise indiscriminate Brownian motion. The effect was demonstrated by older [9,14] as well as very recent experiments [15]. It was amply studied theoretically by direct simulations [16] and using the mapping on one-dimensional diffusion problem [17] based on the Fick-Jacobs theory [18] and its generalizations [19–30]. It turns out that a combination of hydrodynamics and Brownian motion results in phenomena like hydrodynamically enforced entropic trapping [17] and spatially dependent diffusion constant due to hydrodynamic interactions [31].

In these settings, Brownian motion has a decisive role. This somewhat limits the applicability to small enough particles and/or low enough fluid velocity. Beyond this limit there are several approaches which rely purely on hydrodynamics. Perhaps the most straightforward method is sorting by deterministic lateral displacement [32]. A much more delicate method relies on inertial migration, which is based on the Segre-Silberberg effect [33]. Inertial forces induce focusing of the particles at a specific distance from the tube axis [34,35]. In practice, this effect found numerous applications [36–41], notably in blood filtration.

There is a certain dichotomy between microfluidic Brownian ratchets mentioned above and sorting by inertial migration. The former relies on oscillatory flow, but, at least in the studies cited above, in a purely Stokes regime (at zero Reynolds number). The sorting is due to entropic barriers. The latter, on the other hand, relies purely on inertial effects

(the Reynolds number must not be small), but the flow is steady and the sample passes the apparatus in one single run. In a recent paper [42], we combined the two. We showed that in the microfluidic Brownian ratchet the inertial effects are not only important but within some range of parameters they can be even dominant over entropic effects. Here we intend to go even further and show that hydrodynamics alone is sufficient to produce the ratchet effect, even if the Brownian motion is absent (or, more precisely, is infinitesimally small).

The setup we want to investigate closely follows the experiments presented in [9,14]. A spherical particle is carried by periodic flow in a tube of variable diameter. There are at least three length scales in play, resulting in three characteristic Reynolds numbers. The first scale is set by the average tube diameter d and associated to it is the tube Reynolds number $Re_t = Ud/\nu$, where U is the average velocity within the tube, defined through the volumetric flow Q as $U = 4Q/\pi d^2$. Next, there is the scale of particle radius R , and corresponding particle Reynolds number $Re_p = (2R/d)^2 Re_t$. The third scale is the inverse of spatial frequency of tube modulation Ω , and the corresponding Reynolds number $Re_c = \frac{1}{2}\Omega d Re_t$. To fix the typical scales, we can take the values from a standard experiment, e.g., from Ref. [38]. Translating their geometry to our situation, we can consider as typical the values $d = 20 \mu\text{m}$, $R = 1 \mu\text{m}$, $Re_t = 20$, which in turn correspond to $Re_p = 0.2$ and average velocity $U = 1 \text{ms}^{-1}$. Note that the velocity is quite large. Anticipating the value $\Omega d = 0.3$ we shall use most, we get $Re_c = 3$.

Note also that the particle Reynolds number is significantly smaller than the tube Reynolds number. Such a separation of scales justifies a two step approach used in solving the equations for the movement of a spherical particle in the tube.

First, we solve Navier-Stokes (NS) equations for the free flow of the fluid in the tube, assuming that the amplitude of the diameter variations is small. We limit ourselves to the lowest approximations and truncate the expansion of the solution at linear terms in the amplitude.

The approaches to flow in tubes of variable diameter which are available in the literature can be classified in three groups, namely expansion in the slow variation, expansion in the small amplitude of variation, and fully numerical solution.

*slanina@fzu.cz

First, there are results which neglect completely the inertial effects, solving just the Stokes equation. Although they are not much relevant for our purpose, they are useful at least methodically, so we mention them briefly. An interesting exact analytic result [43] shows that in a channel with sharp enough corners, eddies occur inevitably even for slow flow. In approximate analytic calculations either slow-variation [44,45] or small-amplitude [46–48] expansions were used. Fully numerical solutions were also found [49,50].

Now let us turn to results for full Navier-Stokes equations. The expansion in the slow variation was pioneered by Blasius [51]. He considered an exponentially diverging channel and proceeded up to quadratic terms in the speed of variation. The successive corrections to the velocity field are expressed in terms of polynomials of the relative distance from the axis. This method was later widely used for channels and tubes of periodically varying diameter [52–59]. The advantage of this approach consists in the fact that the correction terms have polynomial form, so they can be handled very easily and the expansion can proceed to high orders. However, for us, this type of expansion is not applicable, because we admit the period of spatial variation to be of the same order as the tube diameter, so the variation cannot be described as “slow.”

Instead, we shall use the amplitude of modulation as a small parameter. The expansion in the amplitude of variation was used by Belinfante [60]. He considered a sinusoidally modulated tube and expanded the periodic velocity field in Fourier components. The resulting ordinary differential equations were then solved either in the form of power series or iteratively, in terms of Bessel functions, which physically amounts to the expansion in powers of Reynolds number. However, his solution suffers from the fact that the nonslip boundary conditions are satisfied only up to linear terms in the amplitude of variation and not exactly. This drawback was cured later [61–65], but in these works the ODEs were eventually solved numerically, so no analytical formula resulted. Our goal had been to obtain closed analytical formulas in the first order of the expansion in the small amplitude of diameter variation, with boundary conditions satisfied exactly. We sketched the results of our calculations in our previous paper [42], but without detailed derivation and explanation. Here we present the solution in much more detail and at the same time use the formulas in a completely different regime.

The flow in periodically modulated channels and tubes was also thoroughly studied numerically by different techniques, either assuming stationary and spatially periodic flow [66–74] or solving full time-dependent NS equations [75–81]. The latter group of results is important, because it provides, besides the linear stability analysis [65,71,73,74], an estimate of the critical Reynolds number at which the stationary flow becomes unstable and oscillations first appear. Extrapolating these results to the values of parameters used throughout our calculations, we assume that in our case the critical Reynolds number is not lower than about 200. Therefore, in all our calculations presented below we are safely in a hydrodynamically stable regime.

Finally let us mention that the numerical solutions were often accompanied by direct experimental verification; see, e.g., [66,67,82,83].

With the solution for the free flow at hand, we shall proceed to the second step. Now we insert a spherical particle into the flow. As $Re_p \lesssim 1$, we assume that the perturbation to the flow caused by the particle is given by Stokes equation. The boundary conditions at infinity are fixed by expanding the obtained free fluid flow in the Taylor series around the point where the particle is inserted. In this work, we truncate the Taylor series at quadratic terms, but in principle it is possible to go farther. The procedure of finding the perturbed flow is fairly straightforward and standard [84–87] although we decided to formulate it in our own way which we consider more suitable for future systematic improvements, namely taking higher terms in the Taylor expansion into account. At this point we consider it fair to admit that the method used has a serious limitation. Indeed, it fails if the particle is very close to the tube wall (i.e., the distance is comparable with particle diameter). Close to the wall, more sophisticated methods are necessary, as, e.g., in [88–92]. The effect of wall proximity is not considered here.

In this paper, we aim at closed analytical formulas for the fluid and particle flow. This should enable us to claim that inertial effects lead to a ratchet effect in the movement of the suspended particle and this ratchet effect is a genuine, rather than casual, consequence of mirror-asymmetric tube design.

In fact, the ratchet effect of purely hydrodynamic origin was already demonstrated in numerical simulations [93]. It was found that the particles are sometimes pushed toward the walls, contrary to the naive intuition that close to the wall the velocity of the suspended particle goes to zero, as does the velocity of the fluid. We shall see how this effect emerges from our analytical formulas. Analogous effect was also demonstrated experimentally in a deterministic (i.e., non-Brownian) microfluidic ratchet device [94], composed of triangular, 6- μm large obstacles.

The paper is organized as follows. In Sec. II, formulas for fluid flow in a tube are derived and the limits of their precision (in terms of Reynolds number) are estimated. In Sec. III, the spherical particle is inserted and its movement is calculated. In Sec. IV, the hydrodynamic ratchet is analyzed. Section V draws conclusions from the results presented.

II. SOLUTION FOR THE FLOW IN THE TUBE

The system we shall investigate is depicted schematically in Fig. 1. A Newtonian incompressible fluid of density ρ_f and kinematic viscosity ν is flowing through an axially

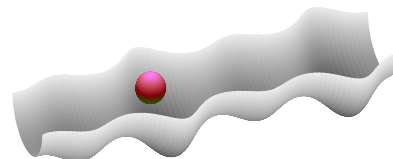


FIG. 1. Schematic picture of the system investigated here. The fluid is flowing through the tube of periodically varying diameter. Within the fluid, there is a colloid particle of spherical shape, whose movement is fully determined (in a nontrivial way) by the movement of the fluid.

symmetrical tube whose diameter changes periodically along the coordinate z directed along the symmetry axis. We shall use the cylindrical coordinates (ρ, z, ϕ) , with a modification which will be explained later. The velocity field of the fluid $\mathbf{u}(\rho, z, \phi)$ is described by Navier-Stokes equations, with usual no-slip boundary conditions at the tube walls. Only axially symmetric solutions (i.e., independent of the azimuthal coordinate ϕ) are considered, so from a technical point of view the three-dimensional (3D) physical situation reduces to an effective 2D problem. This enables the use of the (Stokes) stream function $\psi(\rho, z)$, related to the cylindrical components

of the velocity field as

$$\begin{aligned} u_\rho &= -\frac{1}{\rho} \frac{\partial \psi}{\partial z}, \\ u_z &= \frac{1}{\rho} \frac{\partial \psi}{\partial \rho}. \end{aligned} \quad (1)$$

Then, the continuity equation is satisfied automatically and the Navier-Stokes equation translates in the fourth-order equation for $\psi(\rho, z)$, namely

$$\begin{aligned} & \frac{1}{\nu} \left[\frac{1}{\rho^2} \left(\frac{\partial \psi}{\partial z} \frac{\partial}{\partial \rho} - \frac{\partial \psi}{\partial \rho} \frac{\partial}{\partial z} \right) \left(\frac{\partial^2 \psi}{\partial \rho^2} + \frac{\partial^2 \psi}{\partial z^2} \right) + \frac{1}{\rho^3} \left(\frac{\partial \psi}{\partial \rho} \frac{\partial^2 \psi}{\partial \rho \partial z} - 3 \frac{\partial \psi}{\partial z} \frac{\partial^2 \psi}{\partial \rho^2} - 2 \frac{\partial \psi}{\partial z} \frac{\partial^2 \psi}{\partial z^2} \right) + 3 \frac{1}{\rho^4} \frac{\partial \psi}{\partial \rho} \frac{\partial \psi}{\partial z} \right] \\ &= -\frac{1}{\rho} \left(\frac{\partial^4 \psi}{\partial \rho^4} + 2 \frac{\partial^4 \psi}{\partial \rho^2 \partial z^2} + \frac{\partial^4 \psi}{\partial z^4} \right) + 2 \frac{1}{\rho^2} \frac{\partial}{\partial \rho} \left(\frac{\partial^2 \psi}{\partial \rho^2} + \frac{\partial^2 \psi}{\partial z^2} \right) - 3 \frac{1}{\rho^3} \frac{\partial^2 \psi}{\partial \rho^2} + 3 \frac{1}{\rho^4} \frac{\partial \psi}{\partial \rho}. \end{aligned} \quad (2)$$

Inertial effects are contained in the nonlinear term on the left-hand side. Note that this term is proportional to $1/\nu$. Thus, the presence of the factor $1/\nu$ may serve as a fingerprint of the presence of inertial effects, which will be used later.

We suppose that there are no time-dependent external fields and the fluid velocity is small enough to ensure the stability of time-independent solutions with the same spatial periodicity as the tube itself.

The scheme of Fig. 1 shows also the spherical particle carried by the flow. We assume the sphere is neutrally buoyant, i.e., its density equals the density of the fluid. We also assume that the inertia of the sphere itself is negligible, so that the motion of the sphere is fully determined by the condition that the total force as well as its moment, acting on the sphere, are zero at all times. The influence of the sphere on the fluid flow and the movement of the sphere will be investigated in the next section. Now we shall explain the method we use for calculating analytically the flow of the fluid alone.

A. Expansion in the amplitude of diameter variation

We suppose the fluid flows through an axially symmetric tube with diameter $d/[1 + \lambda S(z)]$ which varies periodically along the tube. We suppose the coordinate axis z coincides with the tube axis and the function $S(z)$ describing the modulation can be expressed in Fourier components as

$$S(z) = \sum_{k=1,2,\dots} (A_k \sin k\Omega z + B_k \cos k\Omega z). \quad (3)$$

We should find a stationary solution for the flow in such a tube. To this end we shall look for the stream function ψ fully describing the axially symmetric flow. We introduce generalized cylindrical coordinates

$$\begin{aligned} \tilde{\rho} &= [1 + \lambda S(z)]\rho, \\ \tilde{z} &= z. \end{aligned} \quad (4)$$

With such coordinates the tube wall is at fixed value $\tilde{\rho} = d/2$, which simplifies the treatment of boundary conditions. For a straight tube the exact solution of NS equations is trivial,

because the inertial term in the NS equations vanishes identically due to the uniformity along the axis, i.e., $\partial \psi / \partial z = 0$. Therefore, the strategy of solution will consist in expansion around this trivial situation. The small parameter of the model is the amplitude of the variation of the tube diameter. This is why we introduced the formal expansion parameter λ , which controls the power in which the variation of the diameter appears in the formula. (As λ is here just for housekeeping purposes, we set $\lambda = 1$ at the end of the calculations.)

So, we write

$$\psi(\tilde{\rho}, \tilde{z}) = \frac{2Q}{\pi} [\psi_0(\tilde{\rho}) + \lambda \psi_1(\tilde{\rho}, \tilde{z}) + \lambda^2 \psi_2(\tilde{\rho}, \tilde{z}) + \dots]. \quad (5)$$

We separated the explicit factor $2Q/\pi$ proportional to the total volumetric flow Q from the rest for further convenience.

The NS equations then lead to a chain of equations for subsequent corrections. Knowing $\psi_0, \psi_1, \dots, \psi_{m-1}$, we obtain linear partial differential equation of fourth order for the next correction ψ_m . In this paper we truncate the expansion at first order in λ , so we calculate just ψ_0 and ψ_1 . The zeroth term can be trivially found as it is formally identical to the standard Poiseuille flow, but expressed in the variable $\tilde{\rho}$

$$\psi_0(\tilde{\rho}) = 2 \left(\frac{\tilde{\rho}}{d} \right)^2 \left[1 - 2 \left(\frac{\tilde{\rho}}{d} \right)^2 \right]. \quad (6)$$

Note that this expression does not contain the factor $1/\nu$, which means that it does not include inertial effects. On the other hand, the corrugation of the tube is already taken into account, although in lowest approximation only.

Knowing ψ_0 , we can write a linear equation for ψ_1 . In analogy to (3), we can expand it into a sum of Fourier components

$$\psi_1(\tilde{\rho}, \tilde{z}) = \sum_{k=1,2,\dots} [\alpha_k(\tilde{\rho}) \sin k\Omega \tilde{z} + \beta_k(\tilde{\rho}) \cos k\Omega \tilde{z}]. \quad (7)$$

Note that at linear level (first order in λ) Fourier components are not mixed and each component is obtained independently

of the others. This simplification is lost if we go beyond the linear approximation, i.e., in calculation of ψ_2 and further terms.

The boundary conditions at the tube wall and at the axis require that

$$\begin{aligned}\alpha_k\left(\frac{d}{2}\right) &= \alpha'_k\left(\frac{d}{2}\right) = \beta_k\left(\frac{d}{2}\right) = \beta'_k\left(\frac{d}{2}\right) = 0, \\ \alpha_k(0) &= \alpha'_k(0) = \beta_k(0) = \beta'_k(0) = 0.\end{aligned}\quad (8)$$

This has an important consequence that the volumetric flow through the tube resulting from ψ_1 is zero, so the total volumetric flow is always Q as given by ψ_0 . Of course, the quantity which is affected by nonzero ψ_1 is the pressure.

We can easily see the following general feature. When we insert (5) into Eq. (2) and rescale all lengths (z as well as ρ) by the spatial frequency Ω , the dimensionless factor

$$\text{Re}_c = \frac{2Q\Omega}{\pi\nu} \quad (9)$$

naturally appears on the left-hand side. This factor will be appropriately called the corrugation Reynolds number, as it measures the importance of inertial effects on the scale determined by the periodic variation of the tube diameter.

Next, performing the linearization of Eq. (2) in the expansion parameter λ , we obtain a linear equation for $\psi_1(\tilde{\rho}, \tilde{z}; \text{Re}_c)$, which depends on Re_c as a parameter. Therefore, any solution can be split into two parts, even and odd in Re_c , respectively, as

$$\begin{aligned}\psi_{1\text{ even}}(\tilde{\rho}, \tilde{z}) &= \frac{1}{2}[\psi_1(\tilde{\rho}, \tilde{z}; \text{Re}_c) + \psi_1(\tilde{\rho}, \tilde{z}; -\text{Re}_c)], \\ \psi_{1\text{ odd}}(\tilde{\rho}, \tilde{z}) &= \frac{1}{2}[\psi_1(\tilde{\rho}, \tilde{z}; \text{Re}_c) - \psi_1(\tilde{\rho}, \tilde{z}; -\text{Re}_c)].\end{aligned}\quad (10)$$

Taking into account the expansion (7) we find that the functions $\alpha_k(\tilde{\rho})$ and $\beta_k(\tilde{\rho})$ can be expressed using a set of functions $g^{(m)}(x; r)$ in such a way that we can write

$$\begin{aligned}\psi_{1\text{ even}}(\tilde{\rho}, \tilde{z}) &= \sum_{k=1,2,\dots} \sum_{l=0}^{\infty} (-1)^l (k \text{Re}_c)^{2l} g^{(2l)}\left(k\Omega\tilde{\rho}; \frac{k\Omega d}{2}\right) \\ &\quad \times (B_k \cos k\Omega\tilde{z} + A_k \sin k\Omega\tilde{z})\end{aligned}\quad (11)$$

and

$$\begin{aligned}\psi_{1\text{ odd}}(\tilde{\rho}, \tilde{z}) &= \sum_{k=1,2,\dots} \sum_{l=0}^{\infty} (-1)^{l+1} (k \text{Re}_c)^{2l+1} \\ &\quad \times g^{(2l+1)}\left(k\Omega\tilde{\rho}; \frac{k\Omega d}{2}\right) \\ &\quad \times (A_k \cos k\Omega\tilde{z} - B_k \sin k\Omega\tilde{z}).\end{aligned}\quad (12)$$

The nontrivial part of the solution is contained in the (still unknown) functions $g^{(m)}(x; r)$.

The equations for these functions are obtained by inserting the expansions (11) and (12) into the NS equations (2) linearized to the first order in λ , and comparing terms with equal power of Re_c , as well as corresponding Fourier coefficients.

In the course of the calculations it appears useful to define the following differential operators:

$$L_1 = \left(\frac{x}{r}\right)^2 \left[1 - \left(\frac{x}{r}\right)^2\right] \left(-x^2 \frac{d^2}{dx^2} + x \frac{d}{dx} + x^2\right), \quad (13)$$

$$\begin{aligned}L_2 &= x^4 \frac{d^4}{dx^4} - 2x^3 \frac{d^3}{dx^3} + (3x^2 - 2x^4) \frac{d^2}{dx^2} \\ &\quad + (-3x + 2x^3) \frac{d}{dx} + x^4,\end{aligned}\quad (14)$$

and the following functions:

$$k_1 = \frac{x^6}{r^4} \left[\frac{8}{r^2} + 1 - \left(\frac{8}{r^2} + 2\right) \left(\frac{x}{r}\right)^2 + \left(\frac{x}{r}\right)^4 \right] \quad (15)$$

$$k_2 = \frac{x^6}{r^2} \left[\frac{16}{r^2} + 1 - \left(\frac{x}{r}\right)^2 \right]. \quad (16)$$

With these objects defined, the NS equations for the stream function transform into the chain of equations for the desired functions $g^{(m)}$, namely

$$\begin{aligned}L_2 g^{(0)} &= -k_2, \\ L_2 g^{(1)} &= L_1 g^{(0)} + k_1, \\ L_2 g^{(m)} &= L_1 g^{(m-1)} \quad \text{for } m \geq 2.\end{aligned}\quad (17)$$

The equations are complemented by boundary conditions

$$\begin{aligned}g^{(m)}(r; r) &= 0 \\ \frac{d}{dx} g^{(m)}(x; r) \Big|_{x=r} &= 0\end{aligned}\quad (18)$$

and

$$\begin{aligned}g^{(m)}(0; r) &= 0 \\ \frac{d}{dx} g^{(m)}(x; r) \Big|_{x=0} &= 0,\end{aligned}\quad (19)$$

which are direct translations of the boundary conditions (8).

As the operator L_2 is of fourth order, a general solution is a linear combination of four linearly independent solutions of a homogeneous equation plus a particular solution due to the right-hand side. However, two of the four solutions contradict the boundary conditions at the center of the tube (19) and only the remaining two independent solutions are applicable. Therefore, the solution will have the following general form:

$$g^{(m)}(x; r) = h_1^{(m)}(r)H_1(x) + h_2^{(m)}(r)H_2(x) + P^{(m)}(x; r), \quad (20)$$

where $H_1(x)$ and $H_2(x)$ are the two independent solutions of the homogeneous equation $L_2\phi(x) = 0$ compatible with the boundary conditions (18) and (19). The values of the two coefficients $h_1^{(m)}$ and $h_2^{(m)}$ are determined by the two equations (18). The terms $P^{(m)}(x; r)$ come from particular solutions. The first one is the particular solution of the equation

$$L_2 P^{(0)}(x; r) = -k_2. \quad (21)$$

Finding the functions $P^{(m)}(x; r)$ for $m \geq 1$ is somewhat simplified by the observation that $L_1 H_1(x) = 0$ and $L_1 P^{(0)}(x; r) + k_1 = 0$. (We do not see any deep reason for

these identities. They just appeared as a result of the calculation.) These identities imply that

$$P^{(m)}(x; r) = \sum_{n=1}^m h_2^{(m-n)}(r) P^{(n,2)}(x; r) \quad (22)$$

and the functions $P^{(n,2)}$ are particular solutions of the inhomogeneous equations

$$\begin{aligned} L_2 P^{(1,2)}(x; r) &= L_1 H_2(x), \\ L_2 P^{(m,2)}(x; r) &= L_1 P^{(m-1,2)}(x; r) \quad \text{for } m \geq 2. \end{aligned} \quad (23)$$

In principle, we can recursively calculate the functions $g^{(m)}(x; r)$ to an arbitrary order. In practice, we used the MAPLE software [95] for finding the solution and stopped at the order $m = 1$, where the inertial effects first appear. The result of this computation (as found using MAPLE) is expressed using the Bessel functions of imaginary argument $I_n(x)$ and $K_n(x)$ (see, e.g., [96]). For the solutions of the homogeneous equation we find

$$H_1(x) = x I_1(x) \quad (24)$$

and

$$\begin{aligned} H_2(x) &= x^2 K_1(x) [x I_0^2(x) - x I_1^2(x) - 2 I_0(x) I_1(x)] \\ &\quad + 2x I_1(x) \int_0^x x' K_1(x') I_1(x') dx'. \end{aligned} \quad (25)$$

The particular solution is very simple in the lowest order, namely

$$P^{(0)}(x; r) = \left(\frac{x}{r}\right)^4 - \left(\frac{x}{r}\right)^2. \quad (26)$$

The coefficients ensuring the satisfaction of the boundary conditions are

$$h_1^{(0)}(r) = -2[K_1(r) + 2I_1(r) \phi_2(r)] \phi_3(r) \quad (27)$$

and

$$h_2^{(0)}(r) = 2I_1(r) \phi_1(r) \phi_3(r), \quad (28)$$

where we defined auxiliary functions

$$\phi_1(r) = \frac{1}{r^2 I_0^2(r) - r^2 I_1^2(r) - 2r I_0(r) I_1(r)}, \quad (29)$$

$$\phi_2(r) = \phi_1(r) \int_0^r x' K_1(x') I_1(x') dx', \quad (30)$$

and

$$\phi_3(r) = \frac{1}{r^2 [K_1(r) I_0(r) + I_1(r) K_0(r)]}. \quad (31)$$

In the first order, the particular solution can be written as

$$P^{(1)}(x; r) = 2x [I_1(x) f_1(x; r) - K_1(x) f_2(x; r)] h_2^{(0)}(r) \quad (32)$$

and the coefficients as

$$h_1^{(1)}(r) = -2[f_1(r; r) + 2 f_2(r; r) \phi_2(r)] h_2^{(0)}(r), \quad (33)$$

$$h_2^{(1)}(r) = 2 f_2(r; r) \phi_1(r) h_2^{(0)}(r), \quad (34)$$

where

$$\begin{aligned} f_1(x; r) &= \int_0^x \int_0^{x'} x' K_1(x') [I_1(x') K_1(y) \\ &\quad - K_1(x') I_1(y)] f_3(y; r) dy dx', \end{aligned} \quad (35)$$

$$\begin{aligned} f_2(x; r) &= \int_0^x \int_0^{x'} x' I_1(x') [I_1(x') K_1(y) \\ &\quad - K_1(x') I_1(y)] f_3(y; r) dy dx', \end{aligned} \quad (36)$$

and

$$\begin{aligned} f_3(y; r) &= \left[\left(\frac{y}{r}\right)^4 - \left(\frac{y}{r}\right)^2 \right] \\ &\quad \times I_1(y) [K_1(y) I_0(y) + I_1(y) K_0(x)]. \end{aligned} \quad (37)$$

This completes the solution of the first two equations in the chain (17).

B. Sample profile

Now let us apply the approximation to a specific example. Let us choose the profile of the tube according to

$$S(z) = A \sin 2\Omega z + B \cos \Omega z \quad (38)$$

and truncate the expansion in powers of Re_c at first order. Collecting all terms, we obtain for the stream function

$$\begin{aligned} \psi(\tilde{\rho}, \tilde{z}) &= \frac{2Q}{\pi} \left\{ 2 \left(\frac{\tilde{\rho}}{d}\right)^2 \left[1 - 2 \left(\frac{\tilde{\rho}}{d}\right)^2 \right] + g^{(0)} \left(\Omega \tilde{\rho}; \frac{\Omega d}{2} \right) B \cos \Omega \tilde{z} + g^{(0)} (2\Omega \tilde{\rho}; \Omega d) A \sin 2\Omega \tilde{z} \right. \\ &\quad \left. + \left[g^{(1)} \left(\Omega \tilde{\rho}; \frac{\Omega d}{2} \right) B \sin \Omega \tilde{z} - 2 g^{(1)} (2\Omega \tilde{\rho}; \Omega d) A \cos 2\Omega \tilde{z} \right] \text{Re}_c + O(\text{Re}_c^2) \right\}. \end{aligned} \quad (39)$$

The first thing to do is to check the accuracy of the analytical approximation (39) against the exact numeric solution. We performed the numerical solution using the COMSOL Multiphysics software. We found that the most critical

region (worst agreement) is where the tube is narrowest, as is naturally expected. We plot in Fig. 2 such a worst-case comparison for the profile we use most often, defined by (38). As expected, the agreement worsens with increasing

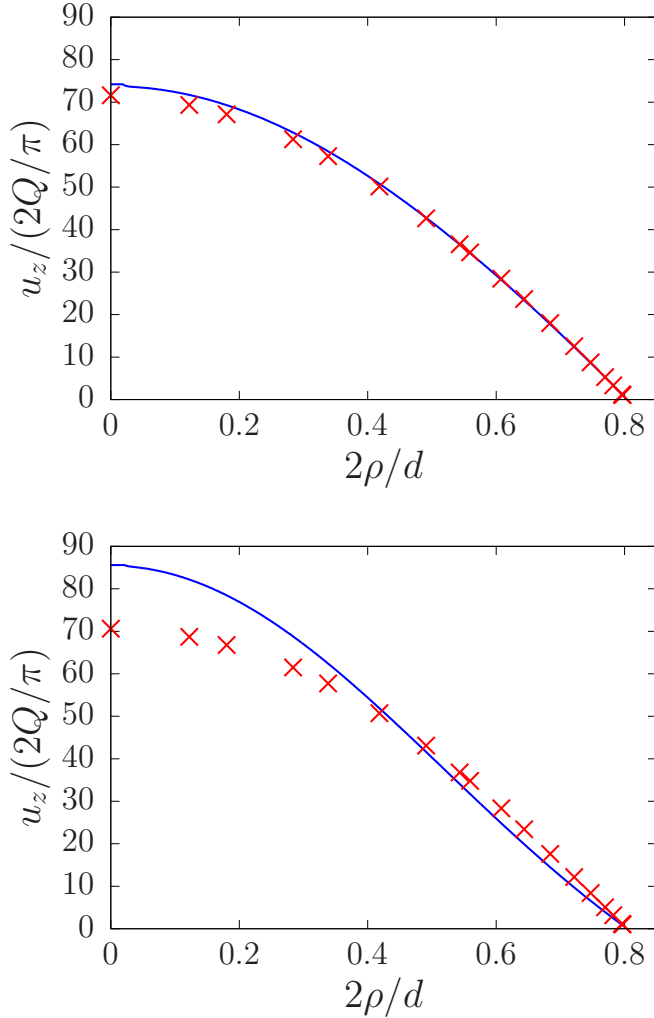


FIG. 2. Comparison of the analytical results based on formula (39) (lines) with exact numerical solution by COMSOL Multiphysics (\times). The profile is defined by (38) with $A = 0.15$, $B = 0.2$, $d = 0.3/\Omega$. In the upper panel, the longitudinal component of the velocity u_z , calculated at the plane perpendicular to the axis at $z = 1/\Omega$, i.e., close to the narrowest profile, for Reynolds number $\text{Re}_c = 4.5$. In the lower panel, the same for $\text{Re}_c = 15$.

Reynolds number. However, the velocity profile for $\text{Re}_c = 4.5$ still agrees very well with the numerics. However, we can see that for example for $\text{Re}_c = 15$ the disagreement is severe, especially at the center of the tube. We observed generally that the disagreement is largest on the tube axis at the narrowest place. This should be expected, as the velocity is largest around there. So, we consider the relative velocity difference $\Delta u_z/u_z = |(u_z^{\text{analytic}} - u_z^{\text{numeric}})/u_z^{\text{numeric}}|$ calculated at $\Omega z = 1$ and $\rho = 0$ as an upper estimate of the error. We show in Fig. 3 how this error bound depends on the Reynolds number. The error of course also increases with increasing A and B . However, we do not consider it reasonable to go beyond the values $A = 0.15$, $B = 0.2$ chosen in Figs. 2 and 3, as the basic assumption of the whole analytical calculations is that the amplitude of the corrugation is small. So, we conclude, on the basis of comparison with exact numerics, summarized in Fig. 3, that our analytical formulas are reliable enough

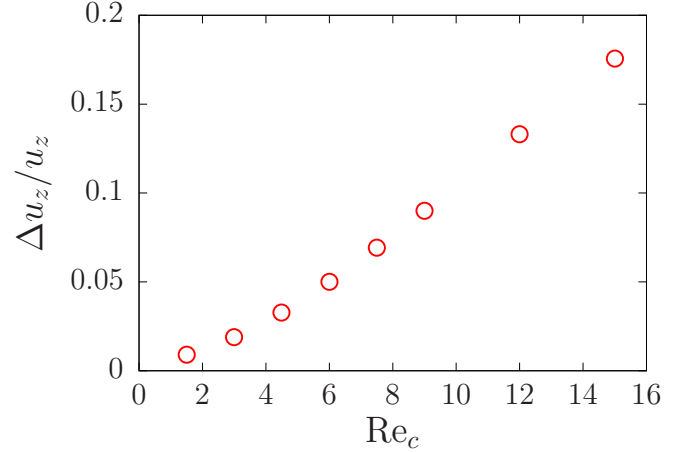


FIG. 3. Comparison of the analytical results based on formula (39) with exact numerical solution by COMSOL Multiphysics. The profile is defined by (38) with $A = 0.15$, $B = 0.2$, $d = 0.3/\Omega$. Here we show how the relative difference between numeric and analytic value of the velocity on the axis (i.e., $\rho = 0$) at the position $z = 1/\Omega$ depends on the corrugation Reynolds number.

for Reynolds numbers $\text{Re}_c \leq 4.5$ and profile parameters $A \leq 0.15$, $B \leq 0.2$.

We illustrate the solution (39) in Fig. 4 showing the streamlines of the flow for two values of the corrugation Reynolds number. (Here and in the following figures, we use $1/\Omega$ as the unit of distance). We can see that if we change the direction of the flow, with all other parameters intact, the shape of the streamlines changes due to inertial effects. We can see it already at the value $\text{Re}_c = 4.5$, up to which the analytical approximation is considered reliable. For pedagogical reasons we also included graphs for larger value $\text{Re}_c = 50$, in order to show how the strength of the inertial effects increases with increasing Reynolds number, although for such large Reynolds numbers the values may not be quantitatively precise enough.

III. PARTICLE IN THE TUBE

A. Spherical particle in ambient flow

Now let us insert a spherical particle of radius R into the computed flow. The particle is considered neutrally buoyant. As a first step, we consider an abstract problem of behavior of a sphere in a given ambient flow. The specific form of the ambient flow is given by Taylor expansion of the flow (39) in powers of the Cartesian coordinates. The origin of coordinates is taken at the point where the sphere center will be placed. This should work for small enough particles and we shall see that this procedure generates indeed an expansion in powers of the radius of the sphere. If we truncate the Taylor expansion at quadratic terms, we obtain correctly contributions up to the order R^2 . So, we suppose the particle is inserted in the flow $\mathbf{u}(\mathbf{x})$ expressed in coordinates as

$$u_i = \beta_i + \beta_{ij}x_j + \beta_{ijk}x_jx_k. \quad (40)$$

(Summation over repeating indices is assumed everywhere.)

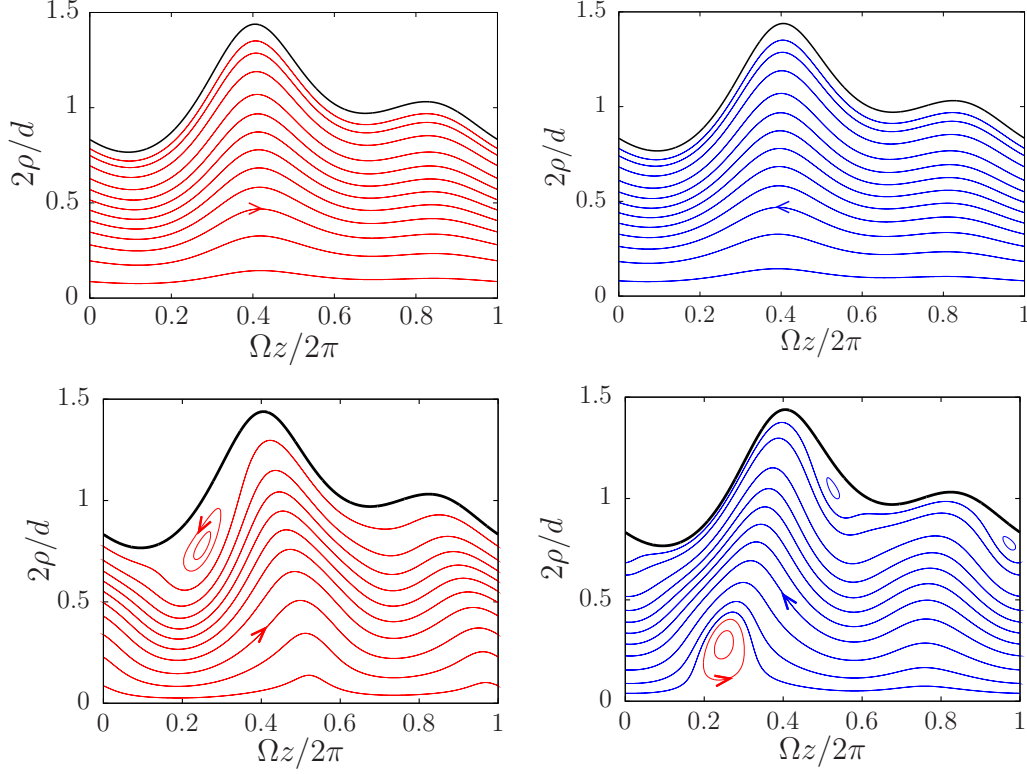


FIG. 4. Streamlines of the flow in tube with profile given by (38), as calculated according to the approximation (39). In the left two panels, the average flow is oriented from the left to the right, while in the right two panels, the orientation is opposite. The Reynolds number is $Re_c = 4.5$ in the top two panels and $Re_c = 50$ in the bottom two panels. The parameters of the tube are $A = 0.15$, $B = 0.2$, $d = 0.3/\Omega$.

The coefficients β_i , β_{ij} , and β_{ijk} must obey certain relations, in order that (40) be a possible solution of Navier-Stokes (NS) equations. First of all, the equation of continuity requires

$$\begin{aligned} \beta_{ii} &= 0, \\ \beta_{iik} &= \beta_{iki} = 0. \end{aligned} \quad (41)$$

Next, the NS equations require the following combinations to be symmetric with respect to exchange of indices $i \leftrightarrow s$,

$$\begin{aligned} &\beta_{il}\beta_{ls} + 2\beta_{isl}\beta_l, \\ &\beta_{il}\beta_{lsk} + \beta_{isl}\beta_{lks} + \beta_{ikl}\beta_{ls}, \\ &\beta_{isl}\beta_{lkm} + \beta_{ikl}\beta_{lsm} + \beta_{iml}\beta_{lks}. \end{aligned} \quad (42)$$

Under these conditions one can determine uniquely the corresponding pressure field $p^{(u)}$ as

$$\begin{aligned} \frac{1}{\rho_f} p^{(u)} &= (-\beta_{il}\beta_l + 2\nu\beta_{ill})x_i - \left(\frac{1}{2}\beta_{il}\beta_{lj} + \beta_{ijl}\beta_l\right)x_i x_j \\ &- \frac{1}{3}(\beta_{il}\beta_{ljk} + \beta_{ijl}\beta_{ljk} + \beta_{ikl}\beta_{ljk})x_i x_j x_k \\ &- \frac{1}{6}(\beta_{ijl}\beta_{lkm} + \beta_{ikl}\beta_{ljm} + \beta_{iml}\beta_{ljk})x_i x_j x_k x_m. \end{aligned} \quad (43)$$

Before we proceed to the calculation of the perturbation caused by the presence of the sphere, we perform an error analysis, comparing the truncated Taylor expansion (40) with the correct flow $\mathbf{u}(\mathbf{x})$, at a distance equal to the diameter

$2R$ of the sphere from the center. We suppose this is the typical distance at which the correction will be significant and therefore errors caused by the truncation of the Taylor series would be important. To estimate the error, we draw a line l_1 parallel to the tube axis at distance $\Delta\rho$ from the axis. At each point on this line we perform the Taylor expansion (40) of the

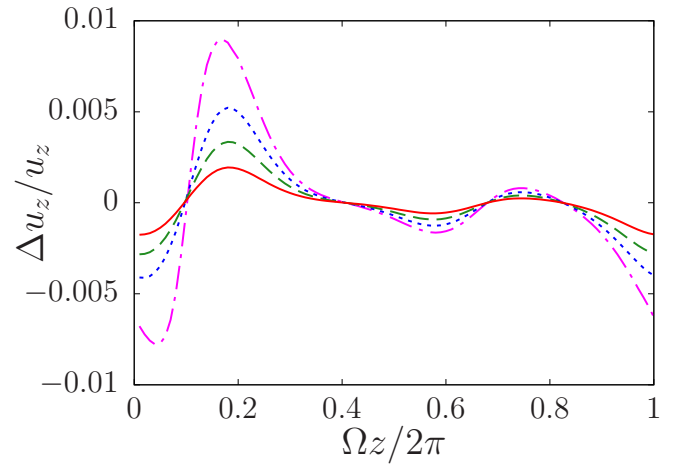


FIG. 5. Relative error due to truncation of the Taylor expansion, for particle radius $R = 0.01/\Omega$, calculated at a line shifted by $\Delta\rho = 0.03/\Omega$ (solid line), $0.05/\Omega$ (dashed line), $0.07/\Omega$ (dotted line), $0.09/\Omega$ (dot-dashed line) from the axis. The profile is defined by (38) with $A = 0.15$, $B = 0.2$, $\Omega d = 0.3$. The Reynolds number is $Re_c = 4.5$.

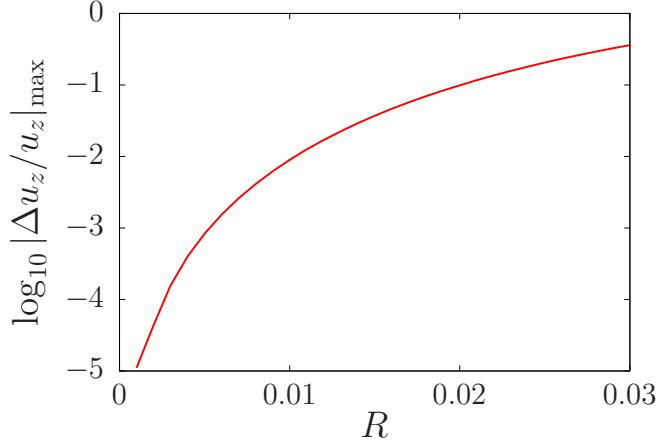


FIG. 6. Maximum relative error due to truncation of the Taylor expansion. The profile is defined by (38) with $A = 0.15$, $B = 0.2$, $\Omega d = 0.3$. The Reynolds number is $Re_c = 4.5$.

flow $\mathbf{u}(\mathbf{x})$ and calculate the axial component of the velocity u_z at a point located by $2R$ farther from the axis, in the direction perpendicular to the axis. At this point we calculate the relative difference between correct and Taylor expanded velocity $\Delta u_z/u_z = (u_z^{\text{Taylor}} - u_z^{\text{correct}})/u_z^{\text{correct}}$. We show in Fig. 5 how the relative error depends on the position on the line l_1 . We can see that if the line is farther from the axis (i.e., for larger $\Delta\rho$) the error increases. Of course, we cannot go with the line l_1 farther from the axis than the particle size allows. We can also see that the error is larger in the narrow regions of the tube, which is due to larger overall velocity and also due to the closeness of the particle to the wall. But in Fig. 5 we can see that for the particle size $R = 0.01/\Omega$ even the maximum error observed (the maximum is taken over all positions along the line l_1 and all shifts $\Delta\rho$ of the line from the axis) is still under 1%. This implies that the truncation of the Taylor series to quadratic terms is well justified. To see how the situation depends on the particle size, we plot the maximum observed error (calculated in the same way as described above), against the particle diameter R . The result is shown in Fig. 6. We confirm that for particles smaller than $R = 0.01/\Omega$ the error is under 1%, but for larger particles the error quickly increases and beyond $R = 0.03/\Omega$ it becomes unbearable.

Now let us turn to the calculation of the perturbation due to the colloid particle. The perturbation to the ambient flow and thus the force acting on the particle can be computed easily as long as the particle is spherical. After insertion of a spherical particle of radius R , the ambient flow $\mathbf{u}(\mathbf{x})$ is modified to $\mathbf{v}(\mathbf{x})$ and we suppose the difference flow $\mathbf{w}(\mathbf{x}) = \mathbf{u}(\mathbf{x}) - \mathbf{v}(\mathbf{x})$ is sufficiently well approximated by a solution of Stokes equation. This can be justified not far from the sphere if the particle Reynolds number $Re_p < 1$ although the tube Reynolds number may be large.

The procedure of obtaining the difference flow $\mathbf{w}(\mathbf{x})$ is standard [84–87] and we sketch it just briefly here. The boundary conditions require that \mathbf{w} vanish at infinity and at the surface of the sphere we have

$$\mathbf{w}(\mathbf{x}) = -\mathbf{u}(\mathbf{x}) \text{ for } |\mathbf{x}| = R. \quad (44)$$

We assume the difference flow can be expressed using an auxiliary vector field $\phi(\mathbf{x})$ as $\mathbf{w}(\mathbf{x}) = \nabla \times \nabla \times \phi(\mathbf{x})$. Then the Stokes equation translates into $\Delta^2 \nabla \times \phi(\mathbf{x}) = 0$. The solution can be found in the form of expansion,

$$\phi_i = \sum_{s=0}^{s_{\max}} \alpha_{ii_1 i_2 \dots i_s} \frac{\partial^s}{\partial x_{i_1} \partial x_{i_2} \dots \partial x_{i_s}} f^{(s)}(\mathbf{x}). \quad (45)$$

The corresponding pressure field will be

$$\frac{1}{\rho_f} p^{(w)} = \nu \sum_{s=0}^{s_{\max}} \alpha_{j i_1 \dots i_s} \frac{\partial^{s+3}}{\partial x_k \partial x_l \partial x_j \partial x_{i_1} \dots \partial x_{i_s}} f^{(s)}(\mathbf{x}). \quad (46)$$

In our case $s_{\max} = 2$. Larger values of s would be necessary, if we took higher terms in the Taylor expansion of the ambient flow (40).

The set of functions $f^{(s)}(\mathbf{x})$ should satisfy the equation $\Delta^2 f^{(s)}(\mathbf{x}) = 0$ and are simply

$$f^{(s)}(\mathbf{x}) = a^{(s)}|\mathbf{x}| + \frac{b^{(s)}}{|\mathbf{x}|}. \quad (47)$$

The problem of finding the difference flow thus reduces to finding the coefficients $\alpha_{ii_1 i_2 \dots i_s}$, $a^{(s)}$, and $b^{(s)}$ such that the boundary condition at the surface of the sphere are satisfied. After lengthy but straightforward calculations we obtain

$$\begin{aligned} w_i = & -\frac{1}{4} \left(\frac{3R}{|\mathbf{x}|} + \frac{R^3}{|\mathbf{x}|^3} \right) \beta_i - \frac{3}{4} \left(\frac{R}{|\mathbf{x}|^3} - \frac{R^3}{|\mathbf{x}|^5} \right) \beta_j x_j x_j - \frac{1}{2} \left(\frac{R^3}{|\mathbf{x}|^3} + \frac{R^5}{|\mathbf{x}|^5} \right) \beta_{ik} x_k + \frac{1}{2} \left(\frac{R^3}{|\mathbf{x}|^3} - \frac{R^5}{|\mathbf{x}|^5} \right) \beta_{ki} x_k \\ & - \frac{5}{2} \left(\frac{R^3}{|\mathbf{x}|^5} - \frac{R^5}{|\mathbf{x}|^7} \right) \beta_{jk} x_j x_k x_i - \frac{1}{8} \left(\frac{2R^3}{|\mathbf{x}|} - \frac{R^5}{|\mathbf{x}|^3} - \frac{R^7}{|\mathbf{x}|^5} \right) \beta_{ill} - \frac{1}{8} \left(\frac{2R^3}{|\mathbf{x}|^3} - \frac{7R^5}{|\mathbf{x}|^5} + \frac{5R^7}{|\mathbf{x}|^7} \right) \beta_{jll} x_j x_i \\ & - \frac{1}{8} \left(\frac{3R^5}{|\mathbf{x}|^5} + \frac{5R^7}{|\mathbf{x}|^7} \right) \beta_{ijk} x_j x_k + \frac{5}{8} \left(\frac{R^5}{|\mathbf{x}|^5} - \frac{R^7}{|\mathbf{x}|^7} \right) (\beta_{jik} + \beta_{kij}) x_j x_k - \frac{35}{8} \left(\frac{R^5}{|\mathbf{x}|^7} - \frac{R^7}{|\mathbf{x}|^9} \right) \beta_{jkl} x_i x_j x_k x_l. \end{aligned} \quad (48)$$

From here we compute the total force acting on the sphere immersed in the flow (40) and its moment with respect to the sphere center. We find

$$\begin{aligned} F_i = & 6\pi\rho_f\nu R \left(\beta_i + \frac{R^2}{3}\beta_{ill} \right) + \frac{4}{3}\pi R^3\rho_f\beta_{il}\beta_l + \frac{4}{45}\pi R^5\rho_f(\beta_{il}\beta_{lmm} + 2\beta_{iml}\beta_{lm} + 4\beta_{ml}\beta_{tim}), \\ M_i = & 4\pi\rho_f\nu R^3\epsilon_{imn}\beta_{nm}. \end{aligned} \quad (49)$$

Here ϵ_{imn} is the totally antisymmetric unit tensor. In our case the particle is freely carried by the flow, and its velocity and rotation are calculated by the transition to moving frame. Indeed, the forces (49) were calculated supposing the sphere does not move. Actually, the sphere moves in such a way that the forces acting on it equal zero (we neglect inertia of the sphere itself). Movement of the sphere with translational velocity s_i and angular velocity ω_i is taken into account by transformation of the coefficients β_i and β_{ij} as

$$\begin{aligned}\beta_i &\rightarrow \beta_i - s_i, \\ \beta_{ij} &\rightarrow \beta_{ij} - \epsilon_{imj}\omega_m.\end{aligned}\quad (50)$$

Inserting the transformed β 's (50) into (49) and equating $F_i = M_i = 0$ we obtain equations for the vectors s_i and ω_i . While the solution for ω_i is trivial and yields

$$\omega_i = \frac{1}{2}\epsilon_{imn}\beta_{mn}\quad (51)$$

the solution for s_i is slightly more complicated, as it requires matrix inversion. To this end we define T_{ij} such that

$$\left(\delta_{im} + \frac{R^2}{9\nu}(\beta_{im} + \beta_{mi})\right)T_{mj} = \delta_{ij}.\quad (52)$$

Then, we obtain for the velocity s_i of the particle

$$\begin{aligned}s_i &= \beta_i + \frac{1}{3}R^2\beta_{ill} + \frac{R^4}{\nu}T_{im}\left(-\frac{4}{135}(\beta_{mk} + \beta_{km})\beta_{kll}\right. \\ &\quad \left. + \frac{2}{135}(\beta_{mkl} + 2\beta_{lmk})(\beta_{tk} + \beta_{kl})\right).\end{aligned}\quad (53)$$

When using these results we must keep in mind that the ambient flow (40) we started with is a truncated Taylor expansion. Including higher terms would result in corrections of order R^4 in Eq. (53). So, to be consistent we can keep just terms to the order R^2 . Therefore, we write

$$s_i = \beta_i + \frac{1}{3}R^2\beta_{ill} + O(R^4)\quad (54)$$

or, in compact notation,

$$\mathbf{s} = \mathbf{u} + \frac{R^2}{6}\Delta\mathbf{u} + O(R^4).\quad (55)$$

We shall use the latter equation in the following computations. In fact, Eq. (55) looks familiar: it is just the Faxén law, because the corrections beyond the R^2 term vanish identically if the ambient flow is governed by the Stokes equation [87]. Note also that although we do not have full formulas for the corrections of the order R^4 , we can infer already on the basis of (53) that the corrections will contain terms nonlinear in \mathbf{u} , so the complexity of the problem rises qualitatively.

B. Inserting sphere in the tube

We shall consider only the axially symmetric flow $\mathbf{u}(\mathbf{x})$ in the tube. From (55) we can see that also the velocity field $\mathbf{s}(\mathbf{x})$, representing the velocity of the particle if its center is exactly at position \mathbf{x} , is axially symmetric. Moreover, the flow $\mathbf{u}(\mathbf{x})$ is incompressible, i.e., $\nabla \cdot \mathbf{u}(\mathbf{x}) = 0$. From (55) it is clear that also $\nabla \cdot \mathbf{s}(\mathbf{x}) = 0$. For any axially symmetric field with zero divergence it is possible to define a stream function. For the velocity field of the fluid it was done in (1). However, an analogous stream function must also exist for the velocity field $\mathbf{s}(\mathbf{x})$, namely, its cylindrical components can be written as

$$\begin{aligned}s_\rho &= -\frac{1}{\rho}\frac{\partial\psi_p}{\partial z}, \\ s_z &= \frac{1}{\rho}\frac{\partial\psi_p}{\partial\rho}.\end{aligned}\quad (56)$$

We shall call the function ψ_p defined by (56) a particle stream function.

The linear relation (55) between $\mathbf{u}(\mathbf{x})$ and $\mathbf{s}(\mathbf{x})$ should induce a linear relation between the corresponding stream functions ψ and ψ_p . To derive such a relation requires some calculations but the final result is fairly simple:

$$\psi_p = \psi + \frac{R^2}{6}\left(\frac{\partial^2}{\partial z^2} + \frac{\partial^2}{\partial\rho^2} - \frac{1}{\rho}\frac{\partial}{\partial\rho}\right)\psi + O(R^4).\quad (57)$$

Note that the differential operator present in (57) is *not* the Laplacian operator expressed in cylindrical coordinates, as one might be tempted to guess simply looking at the form of (55).

Let us take again the specific example of profile (38). The particle stream function then reads

$$\begin{aligned}\psi_p(\tilde{\rho}, \tilde{z}) &= \psi(\tilde{\rho}, \tilde{z}) + \frac{2Q}{\pi}\frac{\Omega^2 R^2}{6}\left\{-32\frac{(1 + A \sin 2\Omega\tilde{z} + B \cos \Omega\tilde{z})^2}{(\Omega d)^2}\left(\frac{\tilde{\rho}}{d}\right)^2\right. \\ &\quad - 4\left[1 - 4\left(\frac{\tilde{\rho}}{d}\right)^2\right]\left(\frac{\tilde{\rho}}{d}\right)^2\frac{B \cos \Omega\tilde{z} + 4A \sin 2\Omega\tilde{z}}{1 + A \sin 2\Omega\tilde{z} + B \cos \Omega\tilde{z}} + 4\left[1 - 12\left(\frac{\tilde{\rho}}{d}\right)^2\right]\left(\frac{\tilde{\rho}}{d}\right)^2\left(\frac{-B \sin \Omega\tilde{z} + 2A \cos 2\Omega\tilde{z}}{1 + A \sin 2\Omega\tilde{z} + B \cos \Omega\tilde{z}}\right)^2\right. \\ &\quad + G^{(0)}\left(\Omega\tilde{\rho}; \frac{\Omega d}{2}\right)B \cos \Omega\tilde{z} + 4G^{(0)}(2\Omega\tilde{\rho}; \Omega d)A \sin 2\Omega\tilde{z} \\ &\quad \left. + \left[G^{(1)}\left(\Omega\tilde{\rho}; \frac{\Omega d}{2}\right)B \sin \Omega\tilde{z} - 8G^{(1)}(2\Omega\tilde{\rho}; \Omega d)A \cos 2\Omega\tilde{z}\right]\text{Re}_c + O(\text{Re}_c^2)\right\} + O(R^4),\end{aligned}\quad (58)$$

where we introduced functions originating from the spatial derivatives,

$$G^{(m)}(x; r) = g^{(m)''}(x; r) - \frac{1}{x}g^{(m)'}(x; r) - g^{(m)}(x; r).\quad (59)$$

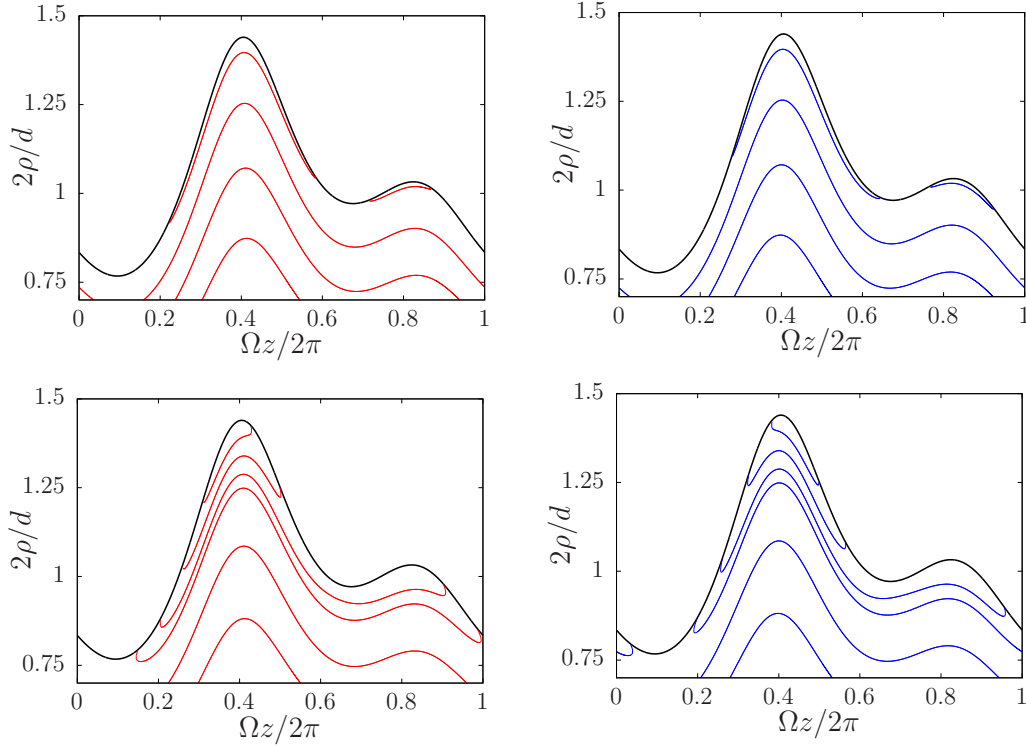


FIG. 7. Streamlines of the flow of spherical particle in tube with profile given by (38), as calculated according to the approximation (58). In the left two panels, the average flow is oriented from the left to the right, while in the right two panels, the orientation is opposite. The Reynolds number is $Re_c = 4.5$. The parameters of the tube are $A = 0.15$, $B = 0.2$, $d = 0.3/\Omega$. The radius of the particle is $R = 0.01/\Omega$ in the top two panels, while $R = 0.03/\Omega$ in the bottom two panels.

(Primes denote differentiation with respect to x .) This result is illustrated in Fig. 7. For particle radius zero the flow would be identical to that of Fig. 4. Nonzero particle size brings a fundamental difference in the flow near the tube walls. Indeed, we can clearly observe in Fig. 7 that there are streamlines which start and end at the wall. For pure fluid flow this is impossible. Here it means that at some places the particle is repelled from the wall (the places where the streamlines emerge from the wall), while at other places the particle is pushed toward the wall (the places where the streamlines end at the wall). This may act as a trap for the particle, in a similar way as the well-known trapping of particles within flow vortices. In a stationary flow, the only way the particle can escape from the trap at a certain section of the wall is Brownian motion. This fact suggests the necessity to include the effects of diffusion even for nominally non-Brownian particles.

IV. HYDRODYNAMIC RATCHET EFFECT

There is another possibility for how to release particles from the wall traps, namely by changing periodically the direction of the flow. The simplest scenario is taking the volumetric flow Q time dependent and periodic, where for simplicity we assume that in the first half period we have $Q = |Q|$ and in the second half period we have $Q = -|Q|$. We suppose the period of the changes is long enough to assure stationary flow within nearly all the duration of each of the two half periods. Thus, we work in adiabatic regime.

Because the tube profile is not mirror symmetric, inertial effects in the flow lead to the asymmetry of streamlines. This asymmetry in turn leads to a difference in the fraction of particles trapped at the wall in the first and second half period. Therefore, also the fractions of flowing particles differ and this results in a net flow of particles in one specific direction, when the flow is averaged over the entire time period. This is the essence of the ratchet effect, well known from the forced diffusion in mirror-asymmetric potentials [12]. Here the ratchet effect is of purely hydrodynamic origin, based on two ingredients. First, there is the trapping effect at the walls, due to the finite size of the colloid particle, and second, there is the inertial effect due to the mirror-asymmetric tube profile and large enough Reynolds number.

To see better how the trapping effect works and how it interferes with diffusion, we performed some numerical calculations using COMSOL Multiphysics software on a schematic model. In fact, for the very existence of the trapping effect it is not crucial that the velocity field of the fluid is a true solution of Navier-Stokes equations. For pedagogical purposes we can equally well use just the zeroth approximation (6). The trapping effect is also completely unrelated to the mirror asymmetry of the tube, so we can use a simple sinusoidal profile

$$S(z) = \frac{1}{2} \cos(\Omega z). \quad (60)$$

The tube we investigate here consists of five periods of the profile (60). We assume the tube connects two reservoirs with uniformly dispersed particles (not shown in the figure).

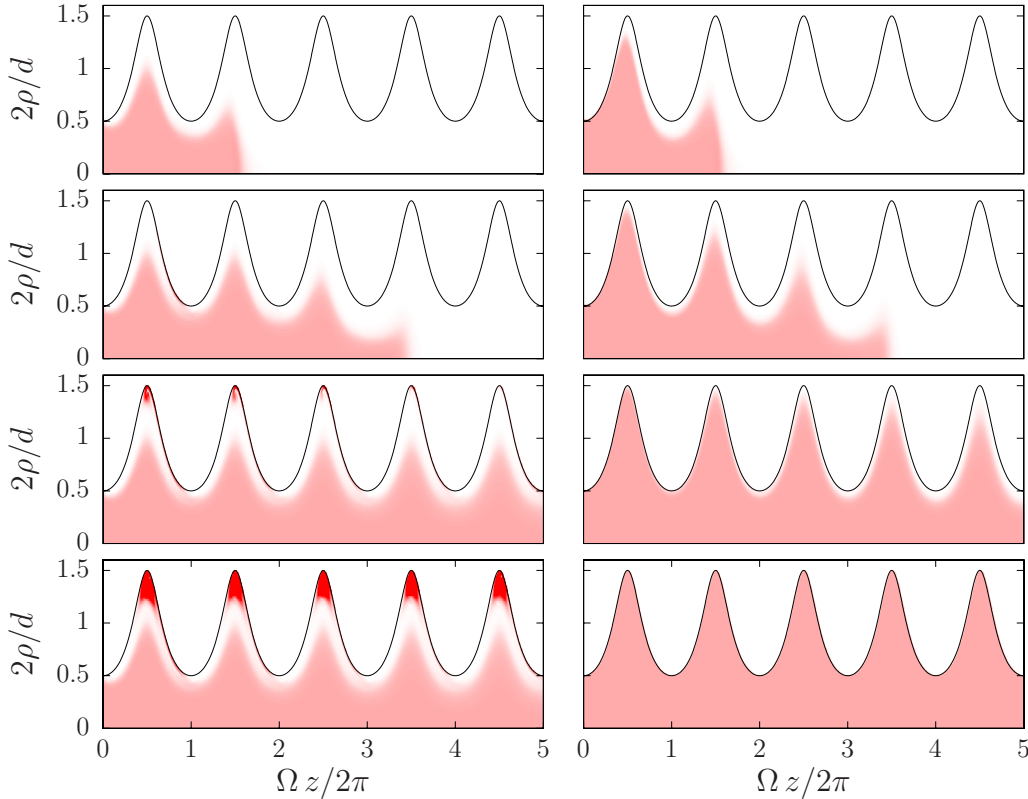


FIG. 8. Time evolution of the concentration of particles under the influence of hydrodynamic drift and very slow diffusion. The data were obtained by numerical solution of advection-diffusion equation using the COMSOL Multiphysics software. The profile of the tube is given by (60). The parameters are $Q = 6$, $\Omega = 10$, $d = 0.3$, diffusion constant is $D_p = 0.0003$. The direction of the flow is from the left to the right. In the left column, the particle radius is $R = 0.05$, in the right column, particle is pointlike, i.e., $R = 0$. In the first three rows, we show snapshots of the concentration at times, from top to bottom, $t = 0.01, 0.02, 0.06$. In the bottom row, we show the concentration in stationary state.

The fluid flow is stationary and defined by the stream function (6). We suppose first that the orientation of the flow is from the left to the right (reversal of the flow will be considered later). The particles carried by the flow move under the influence of drift, according to formula (55), and also by Brownian motion with diffusion constant D_p . As we are interested in the regime of infinitesimally small diffusion, we choose D_p as small as the numerical solution by COMSOL Multiphysics reasonably allows. In practice we used $D_p = 0.0003$. We are interested in the process in which the particles are trapped. To this end, we depict the transient process, where the particles start flowing at time $t = 0$ from the left reservoir and keep uniform and constant concentration at the entrance of the tube, $z = 0$. In Fig. 8 we can see that pointlike particles, whose drift velocity exactly equals the fluid velocity, gradually fill the whole aperture of the tube, starting from the left, and finally reach the stationary state, in which the concentration of particles is uniform throughout the tube. For particles of finite size, the picture is completely different. Already in early stages of the transient, a high concentration of particles builds up at the “dead ends” of the profile, more precisely at the walls, where the tube has maximum diameter. These are the particles trapped by the drift which pushes them toward the wall. At the same time, a layer of finite width along the wall is formed, which, on the contrary, contains few, if any, particles. This is the depletion zone. The remaining volume of the tube is gradually filled by a uniform concentration

of particles. In the stationary state, there are many particles trapped in the “dead ends” and an area of uniform density is bounded inside the area bordered by extremal streamlines. It is easy to understand what are these extremal streamlines, marking a certain “inner tube.” These are the streamlines farthest from the axis, but still neither beginning nor ending at the wall. At most, they may touch the wall at a single point. The existence of such an “inner tube” is crucial, as only through this tube are the particles transported from the left reservoir to the right one.

The existence of finite diffusion complicates to some extent the picture. In a true stationary state, there is a fraction of particles trapped in the “dead ends,” but diffusion allows them to escape, so that the trapped particles are in a dynamical equilibrium. Globally, the same number of particles that enters the tube from the left reservoir leaves the tube into the right reservoir. However, if the diffusion is very slow, it lasts for quite a long time before the stationary regime develops. In the transient regime, the particles are trapped in the leftmost dead ends and keep accumulating there. In the case of infinitesimally slow diffusion all particles are trapped in the first (from the left) period of the tube modulation and the only particles that pass from the left reservoir to the right one are those within the inner tube. Now we should consider alternating the direction of the flow. If the frequency of the alternation is small enough to guarantee stable stationary hydrodynamic flow for the most time, we can apply adiabatic approximation

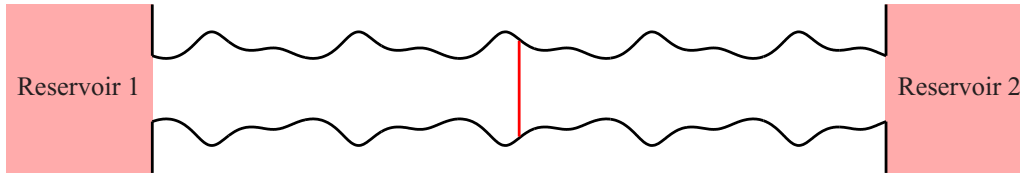


FIG. 9. Schematic picture of a modulated tube connecting two reservoirs, which should serve for rectifying the flow of colloid particles from one reservoir to the other. The numerical simulation is done with exactly this geometry. The reservoirs are implemented by constant (unit) particle density at both entrances and the total particle current is measured at the cross section in exact middle, here indicated by vertical red line.

for the flow. On the other hand, if the frequency of the alternation is large enough compared to diffusion speed, we always remain in the early stages of the transient regime of the trapping effect. Indeed, the particles flowing from the left accumulate first at the leftmost dead end. The only way they can proceed farther to the right is by diffusion. If the direction of the flow changes fast enough, the trapped particles never reach the right end of the tube, but instead, the inverted flow pushes them back to the left reservoir. The same consideration applies symmetrically at the right end of the tube. This means that it is only the inner tube which contributes to the transport of particles between reservoirs in such a regime. Due to the inertial effects the shape and volume carried by the inner tube depends on the orientation of the flow. The number of particles carried by the inner tube from the left to the right differs from the number of particles carried if the direction of the flow is reverted. This is the essence of the hydrodynamic ratchet effect. Let us stress again that this effect occurs only in a certain window of time scales. If we denote the typical transient time to reach the hydrodynamic stationary state T_h and the typical transient time to reach the stationary state due to diffusion T_d , the period T of the alternation of the direction of the flow should fall within the bounds

$$T_h \ll T \ll T_d. \quad (61)$$

The existence of a time scale with such properties requires that the diffusion constant is small enough. Therefore, the regime of hydrodynamic ratchet is the regime of infinitesimally small diffusion.

But the story of time scales does not end here. There are two more time scales related to the geometry of the tube. The first one is the typical time needed for the particle to be transported from one spatial period of the tube modulation to the other. This time is of the order $T_{\text{period}} = 2\pi/(\Omega U) = \pi^2 d^2/(2\Omega Q)$. If $T < T_{\text{period}}$, particles remain within the same spatial period for an extremely long time and there is no ratchet effect at all. But there is an even stronger lower bound on the period T of the modulation. In fact, we assumed that the tube has finite length L and connects two reservoirs with suspended particles. But if the period T is not long enough that the particles are actually transported from one reservoir to the other, they remain “trapped” within the tube, never reaching the other reservoir. Again, the ratchet effect does not take place. This poses an additional bound $T > T_{\text{length}} = L/U = \pi d^2 L/(4Q)$ on the period of alternation.

To see the effect we performed another numerical solution using COMSOL Multiphysics. This time, we chose an asymmetric tube profile according to (38) and the total volumetric

flow was a sinusoidally oscillating function of time. Moreover, we included the inertial hydrodynamic effects into the lubrication approximation (6) in a phenomenological way.

Let us now describe the numerical procedure in more detail. The stream function we use in the numerics has the following form:

$$\psi(\tilde{\rho}, z, t) = q(t)\psi_{\text{pois}}(\tilde{\rho}/d) - \frac{Iq^2(t)S'(z)}{[1+S(z)]^2}\psi_{\text{iner}}(\tilde{\rho}/d), \quad (62)$$

where the time-dependent volumetric flow is $q(t) = Q \sin(\omega t)$ and the spatial dependence of the stream function is decomposed into the bare Poiseuille flow,

$$\psi_{\text{pois}}(x) = \frac{4}{\pi}(x^2 - 2x^4) \quad (63)$$

[this corresponds to (6)], and an inertial correction

$$\psi_{\text{iner}}(x) = x^2 - 8x^4 + 16x^6. \quad (64)$$

The form of $\psi_{\text{iner}}(x)$ is the simplest function satisfying two basic assumptions. First, it produces zero total volumetric flow (so that the volumetric flow is given just by the Poiseuille term) and second, it satisfies the nonslip boundary conditions at the tube wall. The phenomenological constant I measures the strength of the inertial effect and in practical use needs to be fitted so that (62) is the closest possible to the true solution of Navier-Stokes equations. For our purposes I is a free parameter we choose at will. Finally let us note that the factor $S'(z)/[1+S(z)]^2$ comes from the derivative of the tube profile with respect to z and clearly vanishes for a straight tube, where the inertial effects disappear exactly.

With the fluid flow described this way, we studied numerically diffusion of particles of finite radius R . We supposed that the tube connects two equal reservoirs with unit concentration of colloidal particles, as sketched in Fig. 9. The presence of reservoirs is implemented by keeping constant (unit) density of particles at both ends of the tube. The profile of the tube is given by (38). In all numerical calculations we kept the geometry parameters as $d = 0.3$, $A = 0.15$, $B = 0.2$, $\Omega = 10$. The length of the tube was $L = \pi$, so that it contained precisely five periods of the spatial modulation of the diameter. To measure how many particles flowed through the tube, we measured the total flow of particles through the cross section placed in the exact middle of the tube (indicated by the vertical red line in Fig. 9), integrated from the time 0 to t . This integrated current is denoted Q_{int} and provides basic information on the rectification of the colloidal flow, i.e., on the ratchet effect.

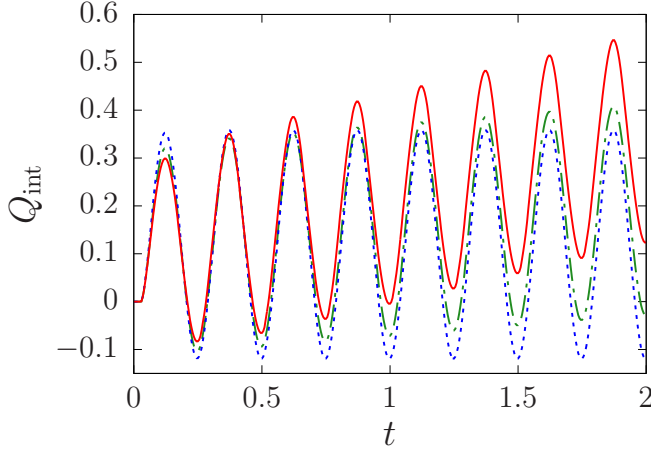


FIG. 10. Integrated current of particles through the cross section in the middle of the tube connecting the two reservoirs, calculated using COMSOL Multiphysics. The geometric parameters of the tube are $d = 0.3$, $A = 0.15$, $B = 0.2$, $\Omega = 10$, $L = \pi$. The amplitude of the volumetric flow is $Q = 6$ and frequency $\omega = 8\pi$. Diffusion constant is $D_p = 0.03$. The remaining parameters are $R = 0$, $I = 0.02$ (dotted line), $R = 0.03$, $I = 0$ (dash-dotted line), and $R = 0.03$, $I = 0.02$ (solid line).

In practical calculations using COMSOL Multiphysics we encountered certain difficulties. Essentially we are interested in the limit of slow diffusion. While the simulations with time-independent flow (Fig. 8) allowed the particle diffusion constant as low as $D_p = 0.0003$, time-dependent flow allowed

where we denoted

$$Q_{p2}(z) = -8 \frac{(1 + A \sin 2\Omega z + B \cos \Omega z)^2}{(\Omega d)^2} - 2 \left(\frac{-B \sin \Omega z + 2A \cos 2\Omega z}{1 + A \sin 2\Omega z + B \cos \Omega z} \right)^2 + g^{(0)''} \left(\frac{\Omega d}{2}; \frac{\Omega d}{2} \right) B \cos \Omega z + 4g^{(0)''}(\Omega d; \Omega d) A \sin 2\Omega z + \left[g^{(1)''} \left(\frac{\Omega d}{2}; \frac{\Omega d}{2} \right) B \sin \Omega z - 8g^{(1)''}(\Omega d; \Omega d) A \cos 2\Omega z \right] \text{Re}_c + O(\text{Re}_c^2). \quad (67)$$

The question is how to understand the z dependence of the nominal particle flow. Of course, the number of particles is conserved. The excess of the flow should be interpreted in terms of particles which are trapped at the tube walls. So, the actual particle flow is given by the minimum of the function (66) over the period of the tube radius modulation. This is just the flow through the inner tube discussed earlier. The value of the minimum depends on the Reynolds number Re_c . If we exchange periodically the flow direction as suggested above, the net flow of particles is given by the difference of minima of the function (66) taken for the same magnitude of Re_c , but opposite sign. We call this net flow ratchet current, and write

$$Q_r = \min_z Q_p(z; \text{Re}_c = |\text{Re}_c|) - \min_z Q_p(z; \text{Re}_c = -|\text{Re}_c|). \quad (68)$$

safely just $D_p = 0.03$ at minimum, otherwise the computation failed to converge (at least with facilities available to us). If the diffusion constant is not small enough, two ratchet effects act simultaneously. There is the ordinary ratchet effect due to entropic barriers [17], as mentioned in the Introduction, and second, there is a purely hydrodynamic ratchet effect due to inertial effects. It is not easy to separate the two, if the diffusion constant is finite, but nevertheless we believe that the inertial effect is still dominant for diffusion constant as large as $D_p = 0.03$ and the geometry described above. We demonstrate this finding in Fig. 10. First, it is clear that for point particles ($R = 0$) the ratchet effect is absent even in the presence of inertial terms. This should be expected, as the point particles follow truly the fluid flow, which is zero after each period of time modulation. If we switch off the inertial terms ($I = 0$) but consider nonzero particle size, we observe small ratchet current due to entropic effects. Then, if we switch on the inertial term, we observe a much stronger ratchet effect. We attribute it to the hydrodynamic inertial contribution.

The essence of the hydrodynamic ratchet explained, let us proceed to a quantitative estimate of the ratchet current. The nominal flow of particles through the tube, which depends on the z coordinate, is equal to

$$Q_p(z) = 2\pi \left[\psi_p \left(\tilde{\rho} = \frac{d}{2}, z \right) - \psi_p(\tilde{\rho} = 0, z) \right]. \quad (65)$$

It can be easily seen that $\psi_p(\tilde{\rho} = 0, z) = 0$, and using the boundary conditions (18) we get the expression

$$\frac{Q_p(z)}{Q} = 1 + \frac{2}{3} \Omega^2 R^2 Q_{p2}(z), \quad (66)$$

We show in Fig. 11 how the position and value of the minima differ when we exchange the direction and that the difference increases when the Reynolds number grows.

We can immediately see from (66) that the ratchet current is proportional to $(\Omega R)^2$. The dependence on the Reynolds number is shown in Fig. 12. In the limit of small Re_c the dependence is linear. (In fact, we found that for even larger Reynolds numbers, not shown in the figure, beyond $\text{Re}_c \simeq 30$, the dependence on Re_c becomes again linear, but with different slope than for small Re_c . However, for such large Reynolds numbers our approximation is unreliable, so we cannot draw any conclusions.) Here we must note that the formula (67) we use for Fig. 12 neglects the terms of order $O(\text{Re}_c^2)$. Therefore, also the nonlinear contribution seen in Fig. 12 is affected by this neglect and just the linear behavior for small Re_c , as seen in the inset of Fig. 12, should be considered reliable.

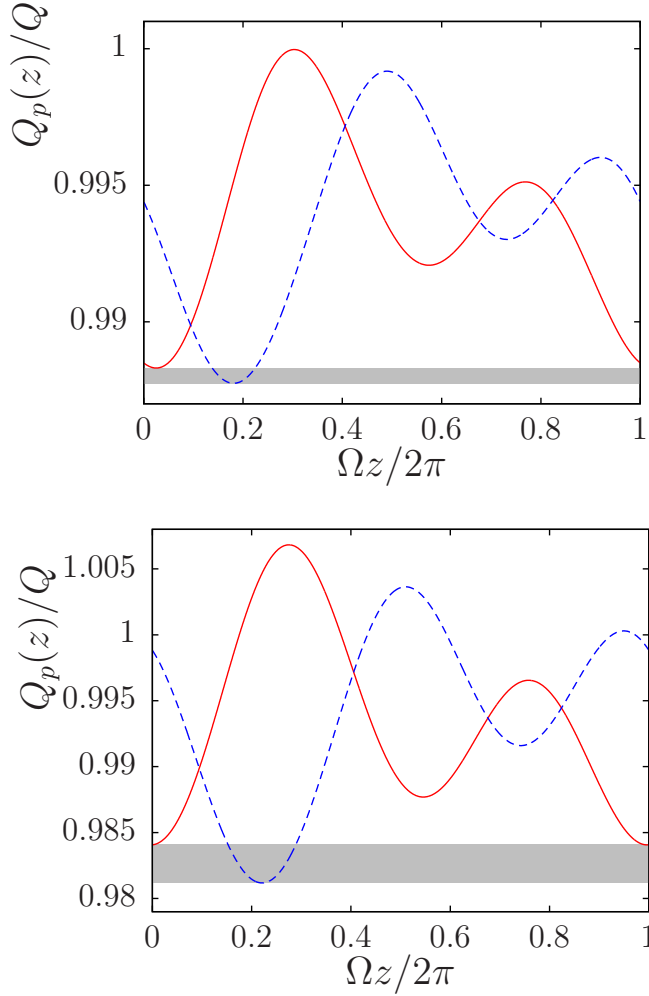


FIG. 11. Nominal particle flow as function of the coordinate z . The parameters of the tube are $A = 0.15$, $B = 0.2$, $d = 0.3/\Omega$. The radius of the particle is $R = 0.01/\Omega$. Solid line corresponds to $\text{Re}_c = |\text{Re}_c|$, dashed line corresponds to $\text{Re}_c = -|\text{Re}_c|$. The magnitude of the Reynolds number is $|\text{Re}_c| = 20$ in the top panel, and $|\text{Re}_c| = 50$ in the bottom panel. The gray shaded area illustrates the difference between the minima, which is proportional to the ratchet current.

We can also see in Fig. 12 that making the tube profile more symmetric, for example by diminishing the coefficient A , results in marked decrease of the ratchet current. On the other hand, the effect of increasing the tube radius, while keeping other parameters intact, makes little difference for small corrugation Reynolds numbers, but decreases the ratchet current when Re_c is large. This is due to the fact that inertial effects are relatively less pronounced in a tube of larger aperture.

To see better the dependence on the profile of the tube, we show in Figs. 13 and 14 the dependence of the ratchet current on the parameters A and B . If either $A = 0$ or $B = 0$, the shape is pure sinusoidal and therefore mirror symmetric. We expect no ratchet effect, and this is confirmed in Figs. 13 and 14. We can also see that typically there is an optimal value of one parameter, if we fix the other parameter. This suggests a way for optimization of the tube profile. Indeed, for a small value of B , e.g. $B = 0.1$, we find optimal A , in

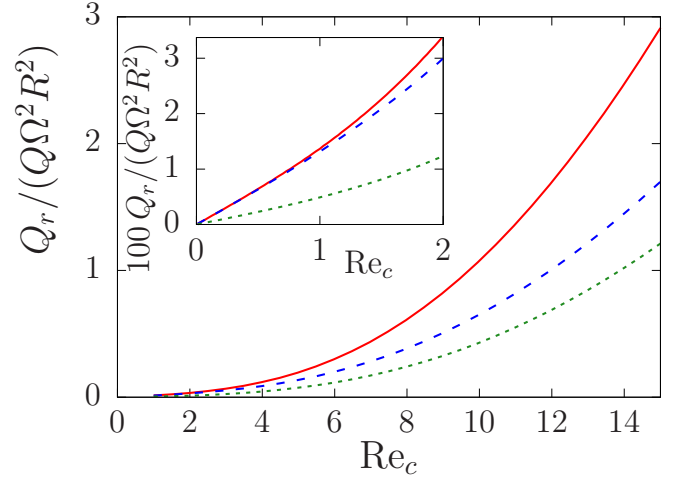


FIG. 12. Ratchet current in adiabatic regime of time-periodic flow. The parameters of the tube are $A = 0.15$, $B = 0.2$, $d = 0.3/\Omega$ (solid line), $A = 0.15$, $B = 0.2$, $d = 0.4/\Omega$ (dashed line), and $A = 0.02$, $B = 0.2$, $d = 0.3/\Omega$ (dotted line).

this example $A = 0.127$, and vice versa. However, this works only for not too high values of the fixed parameter. When we tried to optimize globally (i.e., optimize with respect to both A and B) we found that the globally optimal values of the tube parameters are so high that there hardly remains any free aperture in the tube. This regime surely lies beyond the original and basic assumption of our approximation, that is, that the tube diameter variation is small. This implies that true optimization of the tube profile requires going beyond linear approximation in the corrugation amplitude, and terms of higher order in the auxiliary parameter λ are necessary.

Quadratic dependence of the ratchet current on the particle radius opens the perspective of sorting particles according to their size. Larger particles can move more efficiently and this mechanism provides us with a kind of chromatogra-

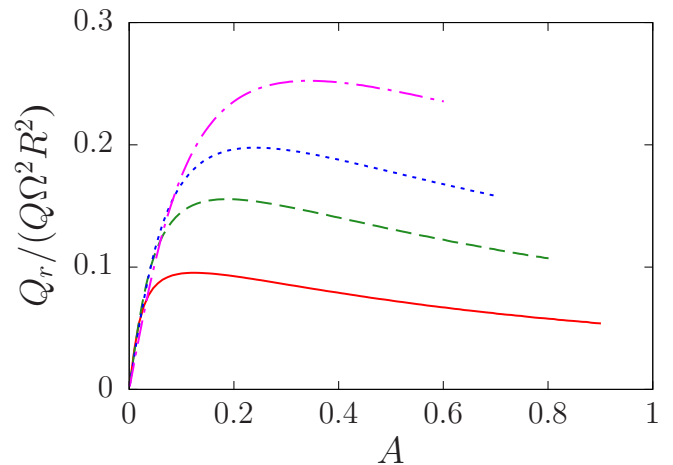


FIG. 13. Dependence of the ratchet current in adiabatic regime of time-periodic flow on the parameter A of the tube profile (38), for $B = 0.1$ (solid line), 0.2 (dashed line), 0.3 (dotted line), and 0.5 (dot-dashed line). The tube diameter is $d = 0.3/\Omega$, the Reynolds number is $\text{Re}_c = 4.5$.

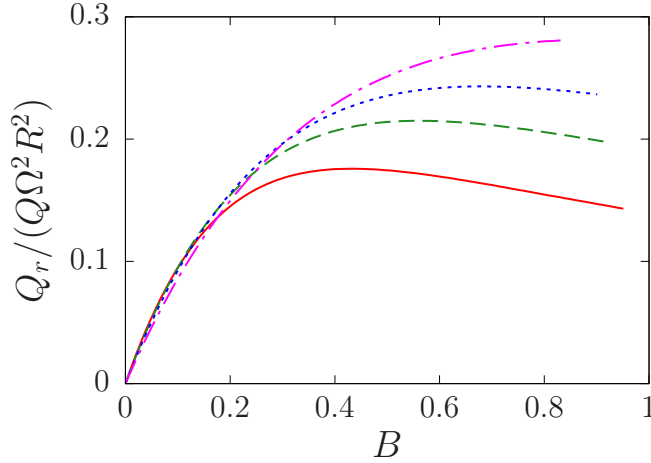


FIG. 14. Dependence of the ratchet current in adiabatic regime of time-periodic flow on the parameter B of the tube profile (38), for $A = 0.1$ (solid line), 0.15, (dashed line) 0.2 (dotted line), and 0.3 (dot-dashed line). The tube diameter is $d = 0.3/\Omega$, the Reynolds number is $\text{Re}_c = 4.5$.

phy, which can separate those larger particles from the rest. In practical use of the hydrodynamic ratchet mechanism it is necessary to assess the inevitable influence of Brownian motion. In all calculations presented here we assumed that the diffusion is infinitesimally small. In fact, smaller particles are more affected by Brownian motion and therefore less efficiently rectified by the hydrodynamic ratchet. But at the same time the ratchet effect itself is proportional to square of the particle radius. Therefore, from this point of view the presence of Brownian motion actually enhances the separation of the large particles from the small ones. Quantitative assessment of the competition between hydrodynamics and diffusion would require much deeper analysis, which goes far beyond the scope of this article and most probably would require numerical simulations, rather than analytical approximations of the kind we are using here. But there is another aspect which complicates the interplay between hydrodynamics and diffusion. In fact, it is possible to achieve particle separation by ratchet effect originating purely from diffusion [23,26]. In fact, in our previous work [42] we briefly sketched how the ratchet effect occurs in a rather special regime, where the fluid velocity is very small but still sufficient to create inertial effects and the diffusion is large enough to create a ratchet effect. (Unfortunately, we did not find any formula interpolating between the regime of strong diffusion used in [42] and the regime of infinitesimally slow diffusion used here.) In a generic situation, the separation of scales $T \ll T_d$ cannot be applied. Both hydrodynamic and diffusion ratchet effects come into play and it is a highly nontrivial question which of them prevails, or rather how they combine together. The regime of infinitesimally slow diffusion investigated in this work is just one of several segments of the parameter space, each requiring separate analysis.

Another complication arises if the separation of scales $T_h \ll T$ is violated. In this regime we must go beyond the adiabatic approximation and solve the time-dependent Navier-Stokes equations. Here we expect complex interplay of non-

stationary diffusion and nonstationary hydrodynamic effects. Clearly, this goes far beyond the scope of the present work.

V. CONCLUSIONS

We found analytical formulas describing the movement of a spherical particle carried by the flow in a corrugated tube. The flow was obtained within the first order in the expansion in the amplitude of the corrugation. We have not checked hydrodynamic stability of the solutions, but in analogy with previous numerical results [76] we believe the results remain stable at least up to Reynolds numbers $\text{Re}_t \lesssim 200$. On the other hand, we compared the analytical results with exact numeric solution of Navier-Stokes equations and we found good agreement (within a few percent) for Reynolds numbers $\text{Re}_c \lesssim 4.5$.

The principal effect we found consists in the fact that the particles are pushed toward the wall at some places and repelled from walls at others. More precisely, the streamlines of the particle flow are not parallel with the tube wall but cross the wall. This may lead to trapping of particles at certain portions of the wall. The trapped particles are immobilized and thus extracted from the flow.

If the profile of the tube is not mirror symmetric, inertial effects induce a difference in streamlines when the orientation of the flux is reversed. Therefore, also the amount of trapped particles is different. This results in the hydrodynamic ratchet effect. This effect occurs when the orientation of the fluid flow is alternated, so that the average fluid flow remains zero. While the fluid does not move on average, the movement of particles is rectified and their current (the ratchet current) is nonzero.

We found that the hydrodynamic ratchet current is proportional to the square of particle radius. Therefore, large particles can be separated from the smaller ones, thus providing an alternative mechanism for particle sorting in colloidal suspensions. In fact, the feasibility of such sorting was already demonstrated experimentally a long time ago [9], although the full theoretical understanding of the experiment is still not entirely complete [14]. We believe the hydrodynamic ratchet effect mechanism studied here contributes to the effect seen in the experiments.

As we already mentioned, the ratchet current is proportional to the square of the particle radius. It also grows with increasing Reynolds number, as expected, because it is due to inertial effects. On the other hand, the dependence on the geometry of the tube is far from obvious. The effect vanishes if the profile is mirror symmetric, but the dependence on the precise shape is nontrivial. This opens the perspective of optimization of the ratchet efficiency by appropriately choosing the tube shape and diameter. However, we found that full optimization of the tube profile would require going beyond the first order approximation in the amplitude of the corrugation.

In the calculation we assumed that the diffusion acting on the particle is infinitesimally small. This assumption was taken in parallel with adiabatic approximation, i.e., the infinitesimally small frequency of alternating the flow direction. So, the results rely on separation of three time scales. The shortest of the three is the time scale of hydrodynamic transient effects. The period of the alternation of the direction of

the flow must be much larger. But the typical diffusion time must be even larger than that.

This raises the question of the interplay between diffusion and hydrodynamic effects, if the time scales are not well separated, i.e., if the diffusion, as well as the frequency, are finite. This goes beyond the methods applied in this work and should be the subject of another study.

As for practical applications of the effect, we can see mainly the sorting of particles according to their size, as already mentioned. However, at this point it is necessary to note that there are several other effects depending on size, which we have not taken into account. First, there is the simple geometric effect, which limits the movement of the center of the particle to an effectively narrower tube, cutting the layer of thickness R at the wall. This effect may dominate the dependence on R , when the condition $R \ll d$ is violated. Also, close to the wall it can be too crude an approximation to truncate the Taylor expansion of the ambient flow at second order. Including higher orders does not pose fundamental problems, just the complexity of the calculation increases.

Next, the very fact that the ratchet effect stems from the behavior not far from the walls calls the effect of hydrodynamic interactions between the particle and the wall into play. This effect was neglected in our calculations, but in principle it could be taken into account using techniques of [88–92] where Stokes flow around spheres at a plane wall is calculated analytically.

Finally, let us mention the technical difficulties which should be expected when we try to go beyond the approxima-

tions used here. First, and most important, is the linearization in the parameter λ measuring the amplitude of the tube corrugation. The main advantage of the linearization was decoupling of the Fourier components in the expansion (7). At the order λ^2 , the stream function can be equally well decomposed in Fourier components, but if we insert it into the Navier-Stokes equations, we find that the components couple with each other. Therefore, we obtain a matrix differential equation for the whole set of Fourier components. This is a much more complicated problem than what was solved in this paper.

The second approximation is the truncation of the Taylor expansion for the ambient flow at second order (40). This induces a correction to the particle flow which is also quadratic in particle size. Next the correction will be of fourth order in particle size and to obtain it we need fourth-order terms in the Taylor expansion for the ambient flow. Calculating the corresponding correction flow around the particle would be rather laborious but essentially identical to what was done at the quadratic level. However, as already noted, a big difference is that the second-order correction to the particle velocity is linear in the ambient flow but the fourth-order correction contains nonlinear terms. This means that the existence of the function we called the particle stream function is not guaranteed and the formalism complicates a lot.

ACKNOWLEDGMENT

The work was supported by the Grant Agency of the Czech Republic, Grant No. 17-06716S.

-
- [1] G. M. Whitesides, *Nature (London)* **442**, 368 (2006).
- [2] T. M. Squires and S. R. Quake, *Rev. Mod. Phys.* **77**, 977 (2005).
- [3] X. Xuan, J. Zhu, and C. Church, *Microfl. Nanofl.* **9**, 1 (2010).
- [4] T. P. Lagus and J. F. Edd, *J. Phys. D: Appl. Phys.* **46**, 114005 (2013).
- [5] P. Sajeesh and A. K. Sen, *Microfluid. Nanofluid.* **17**, 1 (2014).
- [6] J. Xuan and M. L. Lee, *Anal. Methods* **6**, 27 (2014).
- [7] H. Amini, W. Lee, and D. Di Carlo, *Lab Chip* **14**, 2739 (2014).
- [8] T. Salafi, K. K. Zeming, and Y. Zhang, *Lab Chip* **17**, 11 (2017).
- [9] S. Matthias and F. Müller, *Nature (London)* **424**, 53 (2003).
- [10] A. A. S. Bhagat, H. Bow, H. W. Hou, S. J. Tan, J. Han, and C. T. Lim, *Med. Biol. Eng. Comput.* **48**, 999 (2010).
- [11] P. Huber, *J. Phys.: Condens. Matter* **27**, 103102 (2015).
- [12] P. Reimann, *Phys. Rep.* **361**, 57 (2002).
- [13] P. Hänggi and F. Marchesoni, *Rev. Mod. Phys.* **81**, 387 (2009).
- [14] K. Mathwig, F. Müller, and U. Gösele, *New J. Phys.* **13**, 033038 (2011).
- [15] M. J. Skaug, C. Schwemmer, S. Fringes, C. D. Rawlings, and A. W. Knoll, *Science* **359**, 1505 (2018).
- [16] C. Kettner, P. Reimann, P. Hänggi, and F. Müller, *Phys. Rev. E* **61**, 312 (2000).
- [17] S. Martens, A. V. Straube, G. Schmid, L. Schimansky-Geier, and P. Hänggi, *Phys. Rev. Lett.* **110**, 010601 (2013).
- [18] M. H. Jacobs, *Diffusion Processes* (Springer, New York, 1967).
- [19] R. Zwanzig, *J. Phys. Chem.* **96**, 3926 (1992).
- [20] D. Reguera and J. M. Rubí, *Phys. Rev. E* **64**, 061106 (2001).
- [21] P. Kalinay and J. K. Percus, *J. Chem. Phys.* **122**, 204701 (2005).
- [22] P. Kalinay and J. K. Percus, *Phys. Rev. E* **74**, 041203 (2006).
- [23] D. Reguera, G. Schmid, P. S. Burada, J. M. Rubí, P. Reimann, and P. Hänggi, *Phys. Rev. Lett.* **96**, 130603 (2006).
- [24] A. M. Berezhkovskii, M. A. Pustovoit, and S. M. Bezrukov, *J. Chem. Phys.* **126**, 134706 (2007).
- [25] N. Laachi, M. Kenward, E. Yariv, and K. D. Dorfman, *Europhys. Lett.* **80**, 50009 (2007).
- [26] D. Reguera, A. Luque, P. S. Burada, G. Schmid, J. M. Rubí, and P. Hänggi, *Phys. Rev. Lett.* **108**, 020604 (2012).
- [27] A. Ryabov, V. Holubec, M. H. Yaghoubi, M. Varga, M. E. Foulaadvand, and P. Chvosta, *J. Stat. Mech.* (2016) 093202.
- [28] V. Holubec, A. Ryabov, M. H. Yaghoubi, M. Varga, A. Khodae, M. E. Foulaadvand, and P. Chvosta, *Entropy* **19**, 119 (2017).
- [29] P. Kalinay and F. Slanina, *J. Phys.: Condens. Matter* **30**, 244002 (2018).
- [30] P. Kalinay and F. Slanina, *Phys. Rev. E* **98**, 042141 (2018).
- [31] X. Yang, C. Liu, Y. Li, F. Marchesoni, P. Hänggi, and H. P. Zhang, *Proc. Natl. Acad. Sci. U.S.A.* **114**, 9564 (2017).
- [32] L. R. Huang, E. C. Cox, R. H. Austin, and J. C. Sturm, *Science* **304**, 987 (2004).
- [33] G. Segré and A. Silberberg, *J. Fluid Mech.* **14**, 136 (1962).
- [34] J. P. Matas, J. F. Morris, and E. Guazzelli, *Oil Gas Sci. Technol.* **59**, 59 (2004).
- [35] E. S. Asmolov, *Phys. Fluids* **14**, 15 (2002).
- [36] D. Di Carlo, D. Irimia, R. G. Tompkins, and M. Toner, *Proc. Natl. Acad. Sci. U.S.A.* **104**, 18892 (2007).

- [37] J. Seo, M. H. Lean, and A. Kole, *Appl. Phys. Lett.* **91**, 033901 (2007).
- [38] A. A. S. Bhagat, S. S. Kuntaegowdanahalli, and I. Papautsky, *Phys. Fluids* **20**, 101702 (2008).
- [39] M. Masaeli, E. Sollier, H. Amini, W. Mao, K. Camacho, N. Doshi, S. Mitragotri, A. Alexeev, and D. Di Carlo, *Phys. Rev. X* **2**, 031017 (2012).
- [40] J. M. Martel and M. Toner, *Sci. Rep.* **3**, 3340 (2013).
- [41] J. Zhou and I. Papautsky, *Lab Chip* **13**, 1121 (2013).
- [42] F. Slanina, *Phys. Rev. E* **94**, 042610 (2016).
- [43] H. K. Moffatt, *J. Fluid Mech.* **18**, 1 (1964).
- [44] P. K. Kitanidis and B. B. Dykaar, *Transport Porous Media* **26**, 89 (1997).
- [45] D. Bolster, M. Dentz, and T. Le Borgne, *Phys. Fluids* **21**, 056601 (2009).
- [46] J. C. Burns and T. Parkes, *J. Fluid Mech.* **29**, 731 (1967).
- [47] C. Y. Wang, *Phys. Fluids* **18**, 078101 (2006).
- [48] A. E. Malevich, V. V. Mityushev, and P. M. Adler, *Acta Mech.* **182**, 151 (2006).
- [49] C. Pozrikidis, *J. Fluid Mech.* **180**, 495 (1987).
- [50] N. Islam, B. H. Bradshaw-Hajek, S. J. Miklavcic, and L. R. White, *Eur. J. Mech.: B/Fluids* **53**, 119 (2015).
- [51] H. Blasius, *Z. Math. Phys.* **58**, 225 (1910).
- [52] J. H. Forrester and D. F. Young, *J. Biomech.* **3**, 307 (1970).
- [53] M. J. Manton, *J. Fluid Mech.* **49**, 451 (1971).
- [54] J. C. F. Chow and K. Soda, *Phys. Fluids* **15**, 1700 (1972).
- [55] J. C. F. Chow and K. Soda, *J. Appl. Mech.* **40**, 843 (1973).
- [56] K. Vajravelu, *Acta Mech.* **35**, 245 (1980).
- [57] M. Van Dyke, *Adv. Appl. Mech.* **25**, 1 (1987).
- [58] W. P. Kotorynski, *Comput. Fluids* **24**, 685 (1995).
- [59] S. Sisavath, X. Jing, and R. W. Zimmerman, *Phys. Fluids* **13**, 2762 (2001).
- [60] D. C. Belinfante, *Math. Proc. Cambridge Philos. Soc.* **58**, 405 (1962).
- [61] S. Tsangaris and E. Leiter, *J. Eng. Math.* **18**, 89 (1984).
- [62] S. Selvarajan, E. G. Tulapurkara, and V. Vasanta Ram, *Int. J. Numer. Methods Fluids* **26**, 519 (1998).
- [63] H. Zhou, R. E. Khayat, R. J. Martinuzzi, and A. G. Straatman, *Int. J. Numer. Methods Fluids* **39**, 1139 (2002).
- [64] H. Zhou, R. J. Martinuzzi, R. E. Khayat, A. G. Straatman, and E. Abu-Ramadan, *Phys. Fluids* **15**, 3114 (2003).
- [65] E. Abu-Ramadan and R. E. Khayat, *Phys. Rev. E* **75**, 026305 (2007).
- [66] J. A. Deiber and W. R. Schowalter, *AIChE J.* **25**, 638 (1979).
- [67] T. Nishimura, Y. Otori, and Y. Kawamura, *J. Chem. Eng. Jpn.* **17**, 466 (1984).
- [68] M. E. Ralph, *J. Fluids Eng.* **109**, 255 (1987).
- [69] G. Tanda and G. Vittori, *Heat Mass Transfer* **31**, 411 (1996).
- [70] J. Szumbarski and J. M. Floryan, *J. Comput. Phys.* **153**, 378 (1999).
- [71] J. M. Floryan, *J. Fluid Mech.* **482**, 17 (2003).
- [72] H. M. S. Bahaidarah, *Numer. Heat Transfer, Part A* **51**, 877 (2007).
- [73] S. A. Loh and H. M. Blackburn, *Phys. Fluids* **23**, 111703 (2011).
- [74] A. Rivera-Alvarez and J. C. Ordóñez, *J. Fluid Mech.* **733**, 625 (2013).
- [75] I. J. Sobey, *J. Fluid Mech.* **96**, 1 (1980).
- [76] A. Lahbabi and H.-C. Chang, *Chem. Eng. Sci.* **41**, 2487 (1986).
- [77] G. Wang and S. P. Vanka, *Int. J. Heat Mass Transfer* **38**, 3219 (1995).
- [78] K. Stone and S. P. Vanka, *J. Fluids Eng.* **121**, 713 (1999).
- [79] M. Greiner, R. J. Faulkner, V. T. Van, H. M. Tufo, and P. F. Fischer, *J. Heat Transfer* **122**, 653 (2000).
- [80] B. Ničeno and E. Nobile, *Int. J. Heat Fluid Flow* **22**, 156 (2001).
- [81] M. C. Richmond, W. A. Perkins, T. D. Scheibe, A. Lambert, and B. D. Wood, *Adv. Water Resour.* **62**, 215 (2013).
- [82] K. D. Stephanoff, I. J. Sobey, and B. J. Bellhouse, *J. Fluid Mech.* **96**, 27 (1980).
- [83] T. Nishimura, S. Murakami, S. Arakawa, and Y. Kawamura, *Int. J. Heat Mass Transfer* **33**, 835 (1990).
- [84] A. T. Chwang and T. Y. Wu, *J. Fluid Mech.* **67**, 787 (1975).
- [85] A. T. Chwang, *J. Fluid Mech.* **72**, 17 (1975).
- [86] L. D. Landau and E. M. Lifshitz, *Fluid Mechanics* (Butterworth-Heinemann, Oxford, 1987).
- [87] S. Kim and S. J. Karilla, *Microhydrodynamics* (Dover, New York, 2005).
- [88] S. H. Lee, R. S. Chadwick, and L. G. Leal, *J. Fluid Mech.* **93**, 705 (1979).
- [89] S. H. Lee and L. G. Leal, *J. Fluid Mech.* **98**, 193 (1980).
- [90] L. Pasol, M. Chaoui, S. Yahiaoui, and F. Feuillebois, *Phys. Fluids* **17**, 073602 (2005).
- [91] L. Pasol, A. Sellier, and F. Feuillebois, *Q. J. Mech. Appl. Math.* **59**, 587 (2006).
- [92] S. Yahiaoui and F. Feuillebois, *J. Fluid Mech.* **662**, 447 (2010).
- [93] R. L. C. Cisne Jr., T. F. Vasconcelos, E. J. R. Parteli, and J. S. Andrade Jr., *Microfluid. Nanofluid.* **10**, 543 (2011).
- [94] K. Loutharback, J. Puchalla, R. H. Austin, and J. C. Sturm, *Phys. Rev. Lett.* **102**, 045301 (2009).
- [95] www.maplesoft.com.
- [96] N. N. Lebedev, *Special Functions and Their Applications* (Dover, New York, 1972).